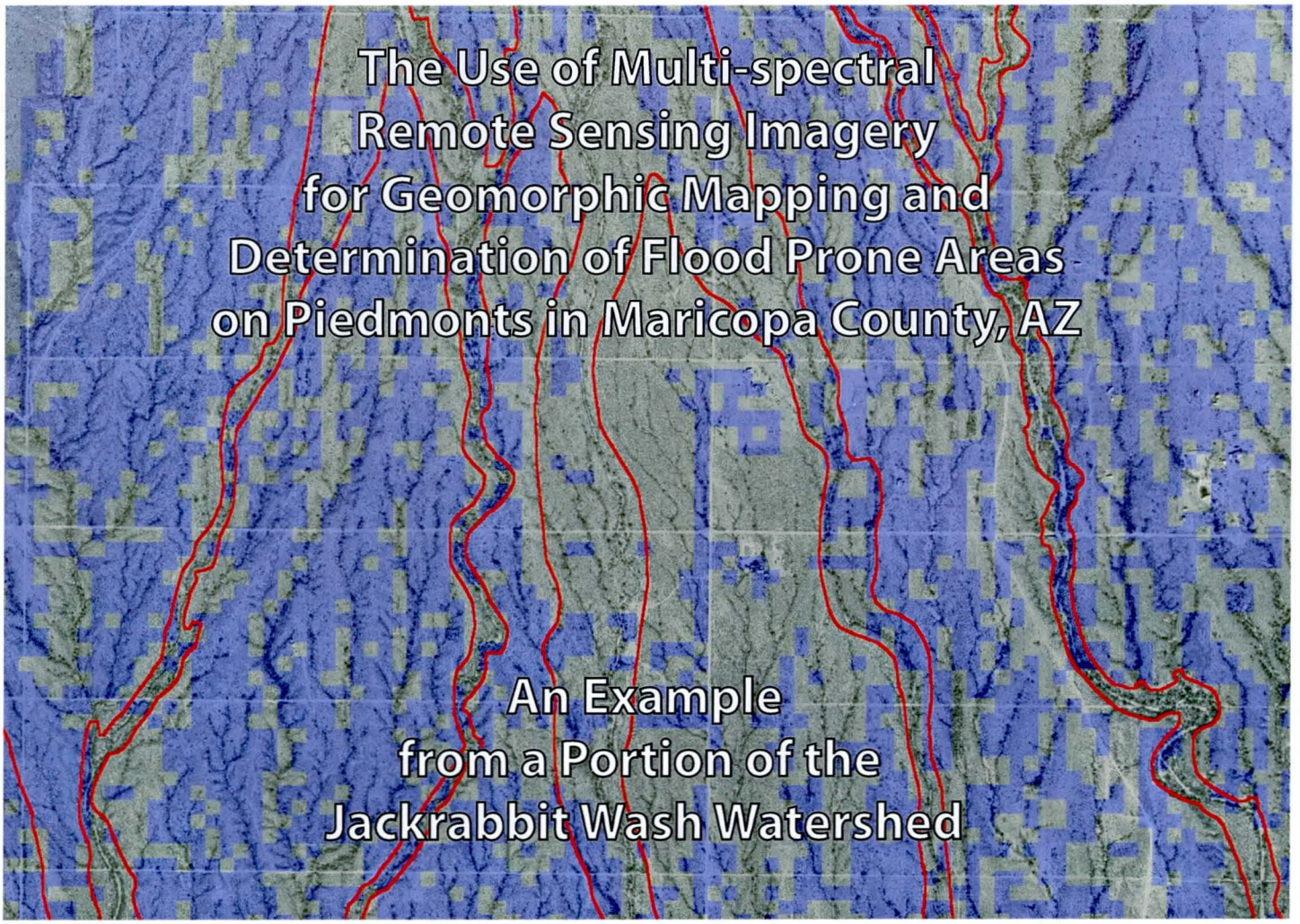

The Use of Multi-spectral Remote Sensing Imagery for Geomorphic Mapping and Determination of Flood Prone Areas on Piedmonts in Maricopa County, AZ

An Example from a Portion of the Jackrabbit Wash Watershed

Report submitted to:
Flood Control District of Maricopa County

FCD 2000C013, Assignment No. 9

Report prepared by:
JE FULLER
HYDROLOGY & GEOMORPHOLOGY, INC.
6101 S. Rural Rd., Suite 110
Tempe, AZ 85283
www.jefuller.com

In association with:
Sarah E. Robinson
Dept. of Geology
Arizona State University

February 2002

Property of
Flood Control District of MC Library
Please Return to
2801 W. Durango
Phoenix, AZ 85009

The Use of Multi-spectral Remote Sensing Imagery For Geomorphic Mapping and Determination of Flood Prone Areas on Piedmonts in Maricopa County, AZ

An Example From a Portion of the Jackrabbit Wash Watershed

Report Submitted to:
Flood Control District of Maricopa County

FCD 2000C013, Assignment No. 9

Report prepared by:
JE FULLER
HYDROLOGY & GEOMORPHOLOGY, INC.
6101 S. Rural Road, Suite 110
Tempe, AZ 85283
www.jefuller.com

In association with:
Sarah E. Robinson
Dept. of Geology
Arizona State University

February 2002

Registered Professional Engineer (Civil)
CERTIFICATE NO.
35895
TED W.
LEHMAN
Date Signed 2/20/02
ARIZONA U.S.A.

Table of Contents

PART ONE: Project Overview 1
Introduction 1
Geomorphic basis for mapping 1
Remote sensing basis for mapping 4
Results 6
PART TWO: Technical Approach 10
General outline of analysis 10
Data selection 10
Preprocessing 11
Image processing 11
Standard band combinations 11
Optimum Index Factor 15
Calculating standard indices 16
Developing scene specific indices 17
Indices calculated specifically for this scene 19
Map generation 20
Expert systems classification 22
PART THREE: Discussion – Lessons Learned 26
Limitations of the study technique 26
Required skill set 27
Comparison of remote sensing results with traditional methods 28
Spatial comparison 29
Level of effort 35
Potential future techniques 35
Topographic analysis 36
Divergence analysis 36
Deconvolution/target transformation 36
Summary and conclusions 36
References 37

Appendix 1. Choosing and ordering data 39
Appendix 2. Data ordered for this project (FCD2000C013, Task 9) 41
Appendix 3. Preprocessing Steps in ERDAS Imagine 43
Appendix 4. Image Processing 50
Appendix 5. Generating Geologic Map 54
Appendix 6. Expert Systems Classification 57
Appendix 7. Additional explanation of some of the standard band ratios 58
Appendix 8. CD-ROM of digital data used and developed in this report 62

Authored by:

Ted Lehman, M.A., P.E., JE Fuller/ Hydrology & Geomorphology, Inc.
Sarah E. Robinson, Arizona State University, Department of Geology
Michael Henze, M.A., JE Fuller/ Hydrology & Geomorphology, Inc.

Registered Professional Engineer (Civil)
CERTIFICATE NO.
35895
TED W.
LEHMAN
Date Signed 2/6/02
ARIZONA U.S.A.

Abstract

Remote sensing analysis of arid region piedmonts can efficiently produce reliable maps of Quaternary geology and geomorphology. Geomorphic maps are a useful resource for floodplain delineation in arid regions as they indicate where floodwater has flowed in the past. The maps are produced through an iterative process of fieldwork and image analysis using Landsat 7 ETM+. A geomorphic map was produced for a northeastern portion of the Jackrabbit Wash watershed in western Maricopa County, Arizona. Our approach used multiple band combinations as backdrops for on-screen digitization and field studies to attach real world characteristics to the digitized units. An expert systems classification was also developed to create a flood prone area map of the study area. This map was compared to 100-year floodplains developed by approximate hydraulic methods used in traditional engineering approaches. The comparison showed variable results. In some areas agreement between the two approaches was good while in other areas they differed greatly. Spatial and temporal resolution differences are most likely responsible for the large variations between the two approaches.

PART ONE: Project Overview

Introduction

Accurately and efficiently mapping the geomorphology of arid piedmonts enhances our ability to map flood hazards in these regions. As population centers in the southwest expand, piedmonts are becoming common targets of development (Gober et al., 2000), requiring evaluation of the flood hazards in these areas. Traditional flood hazard delineation methods rely on hydrologic and hydraulic models in conjunction with topographic mapping. Piedmont flooding is often complicated and unpredictable, resulting in models that do not perfectly predict where water will flow (NRC, 1996). Geologic maps of piedmonts provide information on where water has flowed in the past and can be used in conjunction with traditional methods to improve the accuracy of floodplain delineations.

Assuming that the most recently flooded areas are the most likely to be flooded in the future, geologic information can be used as a basis for flood prone area assessments (Field and Pearthree, 1997). While geologic mapping in arid piedmonts traditionally uses a combination of aerial photographs and fieldwork to delineate geologic units, this project expands the mapping toolkit to include multi-spectral remote sensing datasets. Multi-spectral remote sensing datasets increase our ability to differentiate geologic units, as we are not limited to the color changes recorded in aerial photographs, but can use information about the surface characteristics recorded in parts of the spectrum beyond the visible. Hence, the near-infrared signatures of diagnostic characteristics of geologic units, such as vegetation distributions, clay, and iron can be recorded and located. This project uses multi-spectral remote sensing datasets to develop a geologic map that records the flood history of the region. That geologic map is then used to produce an assessment of flood prone areas in an arid piedmont study site in the Jackrabbit Wash watershed.

Geomorphic basis for mapping

A piedmont is an area of accumulation of sediment eroded from the adjacent mountain front, and may take the form of alluvial fans, channels, and terraces. The sediment is typically deposited by braided streams and/or debris flows (NRC, 1996; Cooke & Warren, 1973). Piedmonts experience cycles of aggradation and incision. Fortunately for geologists, the periods of erosion do not completely remove previously deposited material thereby preserving pockets of deposits from different intervals of deposition (Bull, 1991; Cooke & Warren, 1973) (Figure 1).

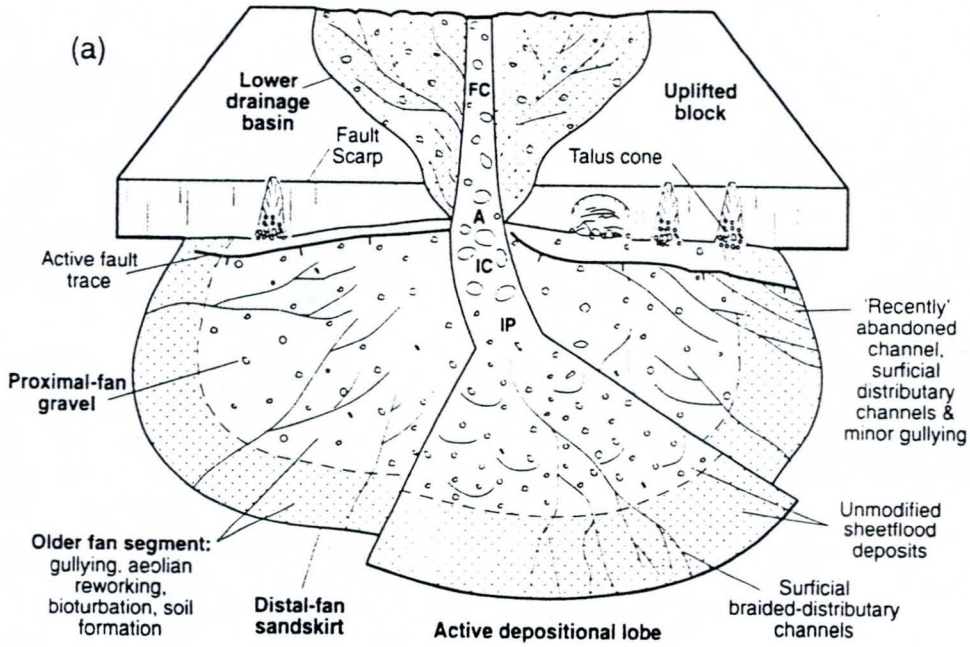

Figure 1. Fluvially dominated alluvial fan (from: Blair and McPherson, 1994)

(A = fan apex, FC = drainage basin feeder channel, IC = incised channel, IP = fan intersection point)

An alluvial fan has active and inactive areas that result from changes in channels' position over time. Active areas are characterized by fluvial and/or debris flow processes that route water and sediment through channels and over adjacent surfaces. In Maricopa County, Arizona, piedmonts and alluvial fans are dominated by fluvial processes. As the channel configuration migrates over the fan surface, or as incision occurs, areas previously prone to flooding become inactive and are changed in character by post-depositional processes. With time, the post-depositional processes change the deposits in a well-documented way and can be used to develop a chronology that documents where water has been in the landscape in the past. (Bull, 1991; NRC, 1996; McFadden et al., 1989).

As areas of deposition are abandoned, bar and swale topography is progressively replaced by a flatter surface covered in by a clast layer, known as desert pavement, formed by mechanical weathering and dust accumulation (Bull, 1991; Cooke & Warren, 1973; Birkeland, 1984). Desert pavement is the armoring of the surface with an increasingly interconnected layer of clasts, one to two clasts deep (Dixon, 1994; McFadden et al., 1997). Clasts with ferrous minerals may also show an association between increasing degrees of pavement development and increasing amounts of iron and magnesium oxide coating (rock varnish) on the clasts (Dorn, 1991; Cooke & Warren, 1973; Bull, 1991). As the subsurface ages, it becomes more stratified with horizons of increasing clay and $CaCO_3$ accumulation. The oldest surfaces may have had their desert pavement stripped and have undergone incision, leaving ridges of calcium carbonate (Birkeland, 1990; Cooke & Warren, 1973) (Figure 2).

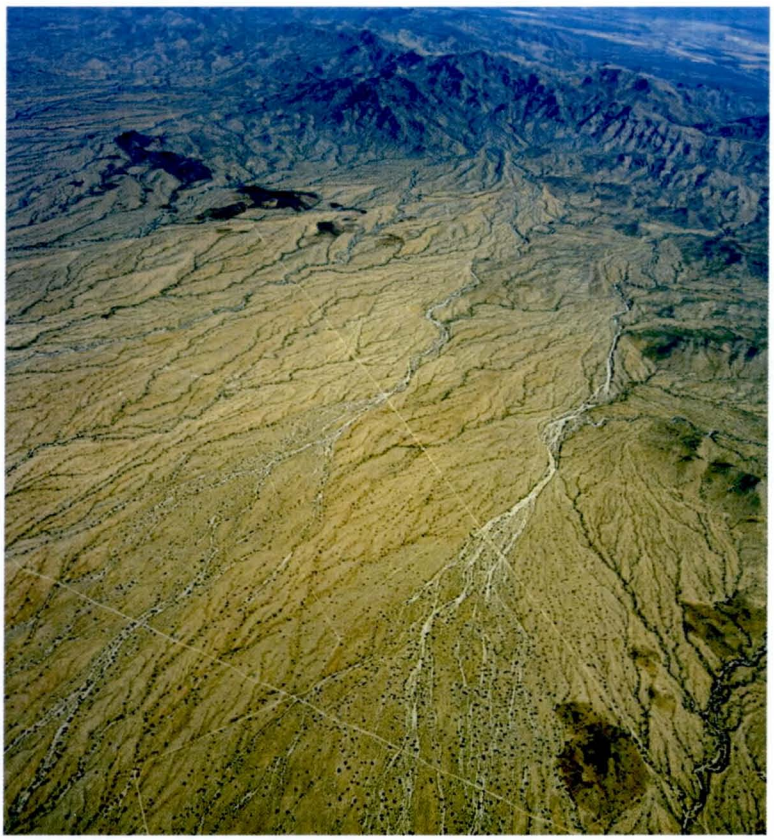

Figure 2. Oblique aerial view of piedmont with various age surfaces

In interpreting the landscape, geologists operate under the well-founded assumption that the presence of post-depositional modifications indicates long periods of inactivity. Thus, a well-developed, varnished pavement or well-developed calcium carbonate layer indicates an area of the fan that has not experienced active fluvial processes for a very long time. Current understanding of the rates of these processes indicates a well-developed, varnished pavement or calcium carbonate layer takes tens of thousands if not hundreds of thousands of years to form (Bull, 1991).

The vegetation communities associated with these deposits also reflect these post-depositional changes in the deposits (McAuliffe, 1994). Specifically, the soil characteristics control soil-moisture which in turn influences the type of vegetation species present. Subsurface characteristics cannot be measured directly with the remote sensing data because the sensors only collect information from the top few microns of the surface. However, the sensor can record the vegetation at the surface. Since vegetation is controlled in part by the subsurface characteristics, vegetation patterns can be used as a proxy for subsurface characteristics.

In desert piedmont environments, the accumulation of clay and carbonate soil horizons change the amount, depth, and variability of soil moisture (McAuliffe, 1994). In unconsolidated gravel deposits, precipitation can infiltrate unimpeded to lower depths. This allows for the storage of water at lower depths, making it less susceptible to evaporation and allows it to be maintained during drought periods. Clay layers and caliche impede the infiltration of water and keep it near the surface where it is more susceptible to evaporation. This results in high soil moisture near

the surface immediately following a wetting, but little to no soil moisture during dry periods (McAuliffe, 1994).

Creosote bush density tends to decrease on Pleistocene deposits with well-developed clay horizons. In contrast, triple leaf bursage and cacti thrive on these deposits, and are typically absent from younger deposits. On the latest Holocene surfaces, creosote is mixed in with other fast-dispersing plants such as burro bush. However, once the creosote becomes established it crowds out these other species and becomes dominant. The density, in addition to the species type, is correlated with the post-depositional changes in these deposits. The development of a desert pavement impedes the establishment of many plants, creating a strong negative correlation with pavement development and plant density.

Post-depositional soil and vegetation characteristics are used by geomorphologists to group deposits with similar histories (i.e. age) into geologic units. These units can then be arranged in a relative chronology from currently active units to units that have been inactive since the early Pleistocene (~1.8 my). Because these post-depositional processes occur only once flooding and sediment deposition have ceased (Field and Pearthree, 1997), the surface chronology can be used as a proxy for a flood history of each mapped unit.

Remote sensing basis for mapping

Remote sensing has been shown in previous mapping studies to be an excellent tool in discriminating between the various Quaternary geologic units in the alluvial fan environment (Farr & Chadwick, 1996; Gillespie et. al, 1984; Robinson and Arrowsmith, in press). Remote sensing data sets span the electromagnetic spectrum from visible to microwave wavelengths. The sensors that produce these datasets measure the energy reflected or emitted by the surface in a particular region of wavelength. The result is a spectrum of the surface which represents the combination of materials present, i.e. vegetation, rocks, soil, etc. (Hunt, 1980; Elachi, 1987).

Traditional Quaternary mapping uses aerial photographs and fieldwork to delineate geologic units. However, aerial photographs restrict the remote sensing information to the visible wavelengths (0.4 to 0.7 microns). Yet, materials absorb, reflect, and emit in all parts of the electromagnetic spectrum. By measuring this interaction at different wavelengths, a unique spectrum or signature of that material is produced (Figure 3). Expansion of the mapping toolkit to include multi-spectral remote sensing data allows for the differentiation of materials that appear similar in the visible spectrum but are actually different.

For example, two different minerals can have the same color in the visible, but their material properties at other wavelengths differentiate them as distinct substances (Figure 4). Clear quartz and calcite may interact with visible light in a similar way giving them the same color, but they do not interact the same way in other parts of the electromagnetic spectrum. Thus, by restricting our "view" to a small part of the spectrum, we limit the number and type of materials that we can discriminate between.

Another advantage of the use of multi-spectral datasets, is that a large area of the earth's surface can be characterized very quickly. Aerial photo interpretation requires a person to examine each area and make a judgment about the nature of the surface characteristics and assign the area to a geologic unit. Computer software can be used to process the multi-spectral datasets to differentiate spectral signatures very quickly.

Figure 3. Example of spectra of different materials

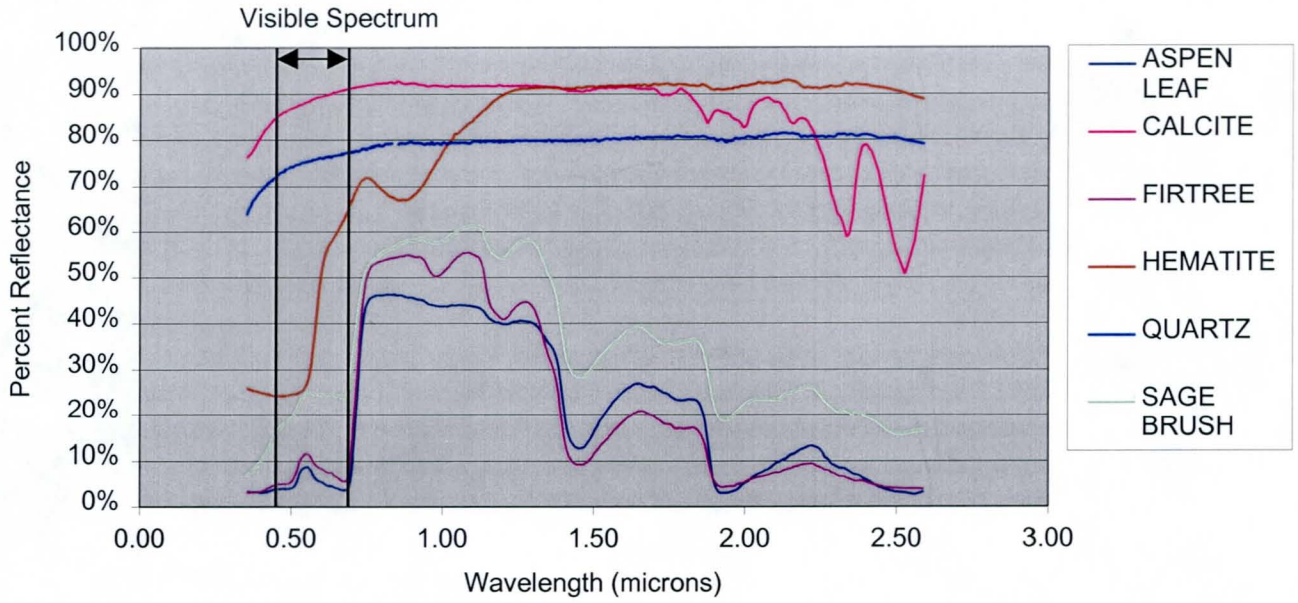

Figure 4. Example of materials that look similar in the visible wavelength region, but different beyond the visible

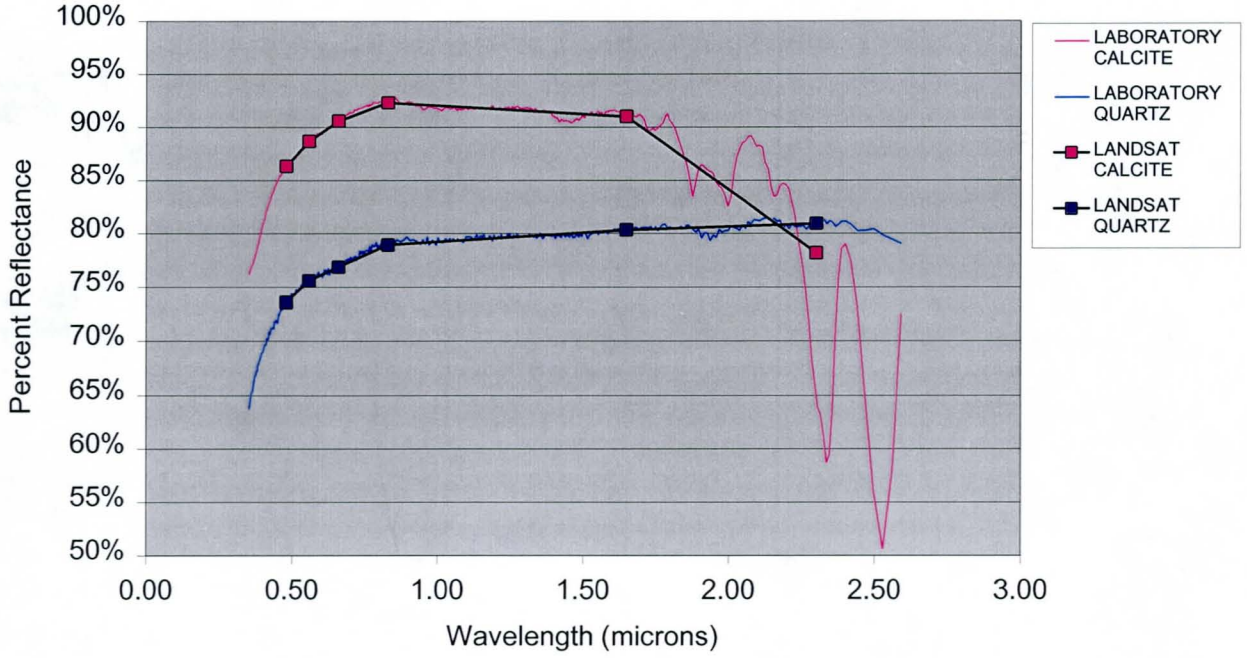

Using multi-spectral datasets to map arid piedmonts assumes that the criteria used to differentiate the units can be "seen" by the dataset. Landsat data only record the interaction of the incident energy with the top few microns of the surface material. Thus, if deposits could be distinguished solely on the presence or absence of a soil horizon one meter below the surface, but were in all other respects identical, the Landsat data could not be used to differentiate them. However, as discussed above, the landform surficial characteristics do change with age. Surface changes include reddening of the soil, development of desert pavement and rock varnish, and changes in vegetation types and density. Since surficial criteria can be "seen" by Landsat, the Landsat dataset can be use to discriminate these units based on some of the same criteria used by field geologists.

Results

A geologic and a flood hazards map were developed for this project. The flood hazards map was produced using an expert classification system, based on the geologic map. The geologic map was created through on-screen digitization on top of multiple remote sensing band combinations images (Figure 5). The processed images were taken into the field and used to identify field sites that were representative of each map unit. At each site, the surface characteristics were recorded and photographed. Additionally, at some sites, soil pits were dug to ascertain sub-surface soil characteristics. A total of nine geologic units were identified. The characteristics, geologic and flood hazard interpretations of the units are given in Table 1. Finally, the field-verified expert system classification developed during this project was used to create a map of flood prone areas for the entire study area (Figure 6).

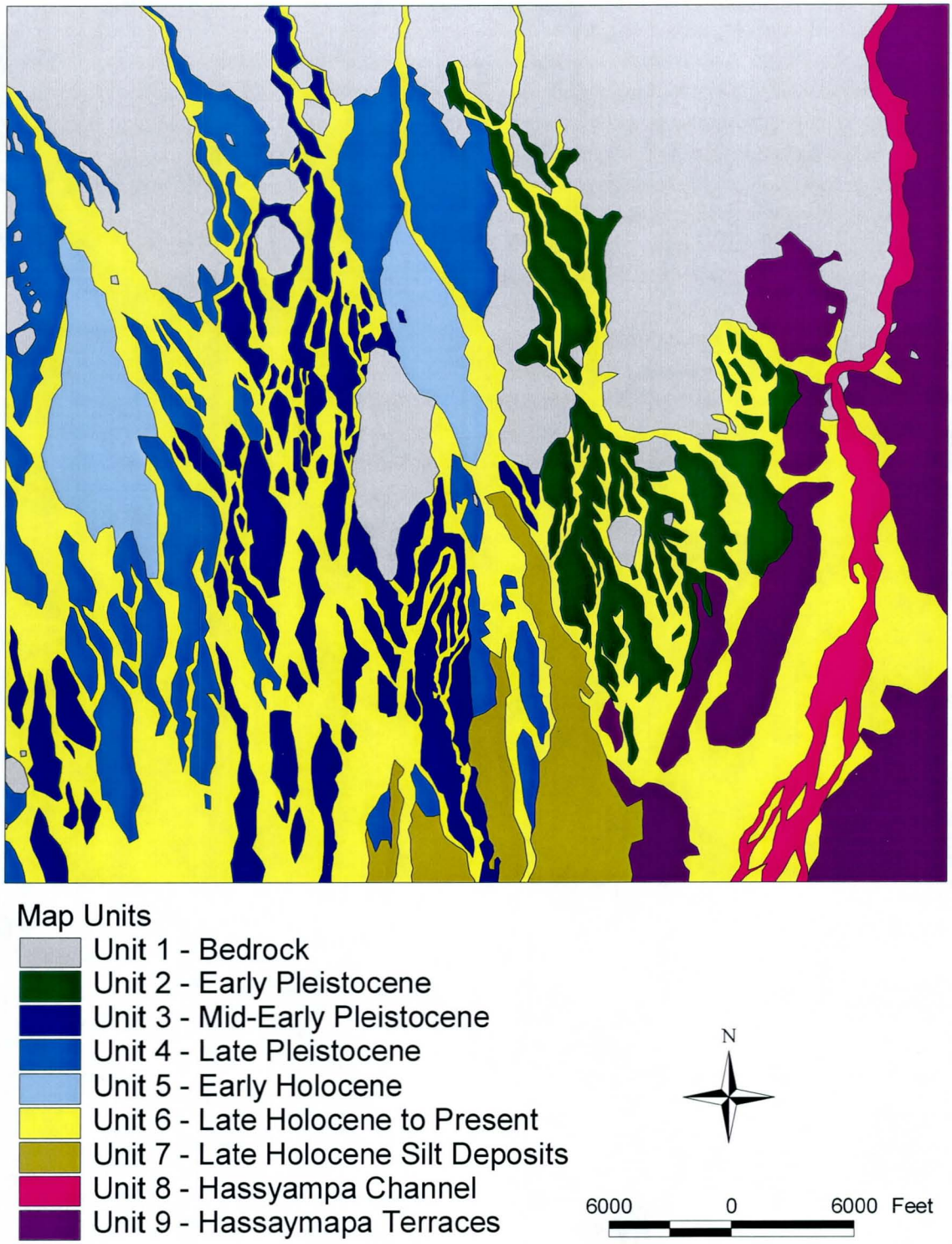

Figure 5. Geologic Map Developed From Landsat Data

Table 1. Description of Geomorphic Map Units Shown in Figure 5

	Geologic Field Observations:	Unit Interpretations	
		Geomorphic	Flood Hazard
Unit 1	Bedrock – outlines taken from geologic map (Dempsey, 1988)	Mountains and hillslopes	Hillslope runoff
Unit 2	Topographically high unit with flat-lying central portions sloping into incising channels, typically forming a dendritic pattern. There are patches of well-armored areas with a 50-70% clast cover and areas that are clast poor with a 30% clast cover. These well-armored patches are typically in the center of the units away from the incising channels. The soil is reddish with an AV horizon and underlying clast free zone. The vegetation is widely spaced with 3-4 m diameter clearings. The vegetation present includes saguaro, teddy bear cholla, creosote and some patches of annual grasses.	Early Pleistocene unit	Unlikely to be inundated
Unit 3	Characterized by moderate to well-developed pavement, but little to no varnish. Clasts cover 40 –70% of the surface and the soil is gray to tan with little red color. The clasts are small to medium (2 to 5 cm). There are patches of well-developed pavement interspersed with patches of poorly developed pavement. These poorly developed areas are often associated with vegetation or local topographic lows. The vegetation present includes teddy bear cholla, creosote, saguaro and sparse annual vegetation. Broad expanses of well-developed pavement have little to no vegetation (3-4 m diameter areas)	Mid-Early Pleistocene unit	Unlikely to be inundated
Unit 4	Characterized by moderately developed pavement with a bimodal distribution of clasts with one group measuring 2-5 cm and a second group measuring 10+ cm. Annuals are present but are not ubiquitous. Large areas are vegetation free (1-2 m diameter). Vegetation is widely spaced (2-3 m apart) and includes creosote, teddy bear cholla, saguaro, brittle bush and some annuals.	Late Pleistocene unit.	Infrequent inundation
Unit 5	Characterized by incipient clast lag development with varying degrees of bar and swale topography preserved. Vegetation species include creosote, bursage, and annuals.	Early Holocene unit	Localized areas of both frequent and infrequent inundation
Unit 6	Characterized by no clast lag present at surface, no sorting of clasts, and little to no soil development. Bar and swale topography still present with larger clasts (15-20 cm) preferentially located on bars. Annual grasses are dominant with no bare patches larger than a few centimeters. Other vegetation present includes creosote and bursage, with creosote being dominant. Cacti are absent or sparse. This unit includes active piedmont channels with dense vegetation typically dominated by palo verde.	Holocene unit	Frequent inundation
Unit 7	Silt dominated surface with no clast lag present. Vegetation is typically exclusively creosote widely spaced (2-3 m apart).	Holocene overbank flood or sheet wash deposits	Frequent inundation
Unit 8	Sand and gravel dominated channel with no soil development and no sorting of clasts. Almost complete absence of vegetation.	Hassayampa River Active Channel	Frequent inundation
Unit 9	Topographically high unit that borders Hassayampa River active channel. Cemented with caliche in subsurface with sub-rounded to rounded cobbles on surface.	Hassayampa River Terrace	Unlikely to be inundated

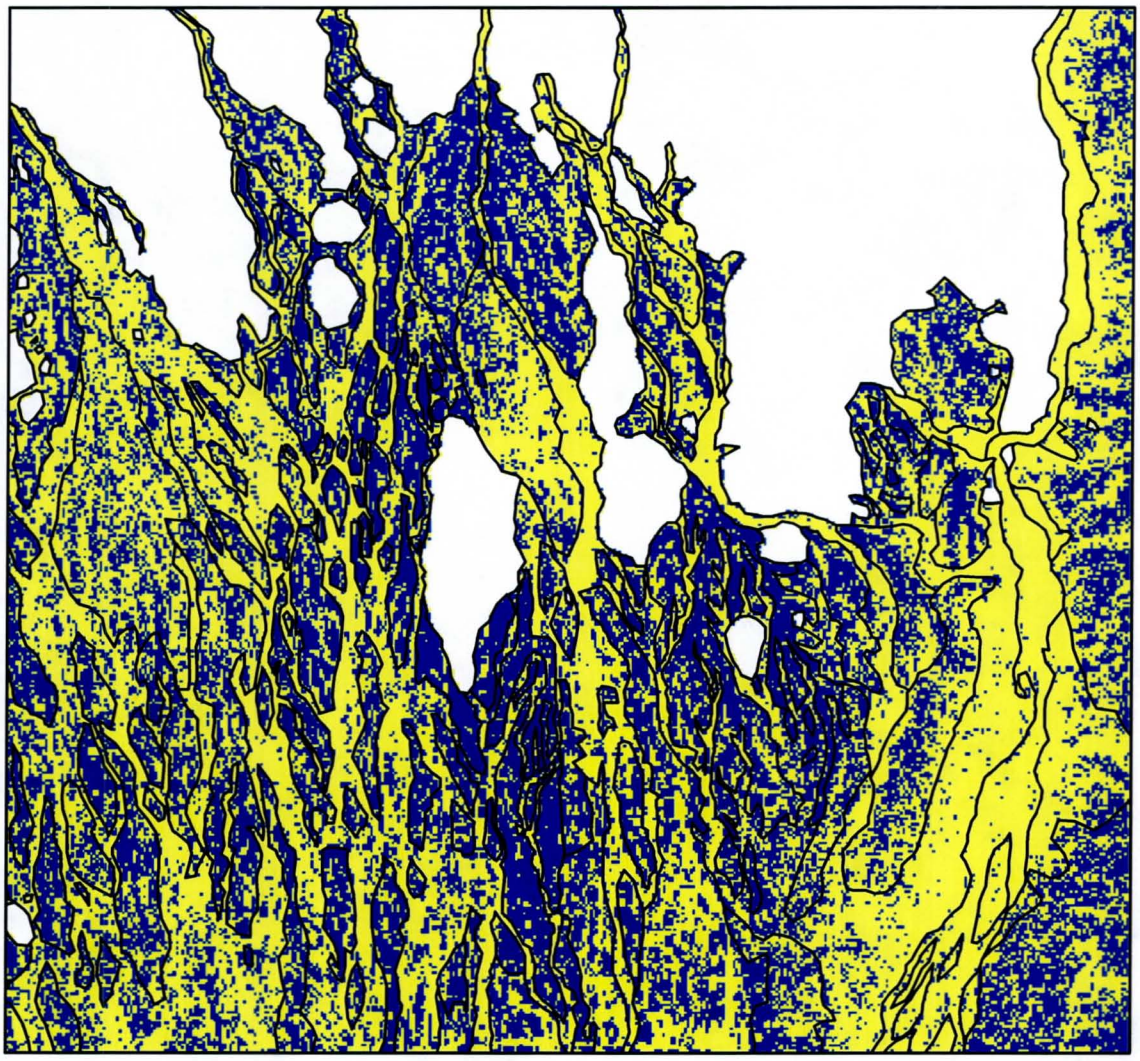

Legend

- Bedrock
- Not flood prone
- Flood prone

Black lines are unit boundaries shown in Figure 5.

N

6000 0 6000 12000 Feet

Figure 6. Flood Prone Areas Derived From Landsat Data

PART TWO: Technical Approach

General outline of analysis

The goal of this project was to produce a geologic map of an arid piedmont and use this information to identify flood prone areas. The resulting flood prone area map was then compared to identification of flood prone areas by conventional engineering methods. The steps of this project are summarized in the following outline.

- Select the appropriate data for the project goals
- Perform preprocessing that generates atmospherically corrected and georeferenced data
- Perform image analyses
- Collect field data to attach real world characteristics to these images
- Create geologic map through on-screen digitizing
- Develop an expert classifier that automates the mapping
- Develop a flood prone areas map from the geomorphic map
- Compare the satellite-derived flood prone areas with those from the in-progress Jackrabbit Wash Approximate Floodplain Delineation Study (JEF, in-progress). The comparison is presented in Part Three.

Data selection

The two basic discriminators in remote sensing data sets are spectral and spatial coverage. Spectral coverage refers to the region of the electromagnetic spectrum in which data are recorded and how many bands are measured in that region. The appropriate region of the electromagnetic spectrum is selected based on the surface materials in the scene and the goals of the project.

In addition to spectral characteristics, each remote sensing dataset also has a particular pixel resolution and spatial coverage. Sensors flown on aircraft have smaller pixel sizes (1 m to 30 m) while those flown on satellites have much larger pixels (30+m) due to the higher orbit altitude. Satellite sensors have the advantage of covering large areas and taking multiple images of the same location. For example, Landsat covers every location on the globe, every 16 days. In contrast, aircraft sensors have sporadic ground coverage as they are only flown over requested areas.

Landsat 7 ETM+ was selected as the primary multi-spectral data source for this project because it met the spectral needs of this study and is an easily accessible, readily available dataset. Landsat ETM+ has bands specifically selected in the short wave infrared spectrum to record information about vegetation, hydroxyl-bearing minerals, and iron rich materials; all indicators of the post-depositional processes used to differentiate the geologic units (Sabins 1997). Furthermore, Landsat has become a standard remote sensing dataset. Any technique proven to be effective using this data is easily extrapolated to other regions of interest. More detailed information is available on the Landsat website:
http://ltpwww.gsfc.nasa.gov/IAS/handbook/handbook_toc.html.

Analysis of other types of data was also part of the original proposal. However, ASTER data were not available for the study area until late last fall and therefore was not included in this study to accommodate the project schedule. Radar data were ordered to evaluate surface roughness and particle size, both of which are linked to desert pavement development. However,

those data required intensive processing and remote sensing knowledge reaching the level of effort for traditional floodplain delineation methods. Additionally, the resolution of the radar data was too large to provide information on the smaller channels of interest.

Software used:
The image analysis in this study was performed using the ERDAS Imagine image processing software package. ArcINFO and ArcView were also used in the generation of the geomorphic map. ERDAS Imagine was chosen because of the mapping nature of this project and this program's compatibility with the GIS software used. However, any of the currently available image processing packages (ENVI, ERMapper, etc.) can perform the entire suite of image processing techniques used in this study.

Preprocessing

The preprocessing of the Landsat scene[1] included subsetting the study area from the larger 150 km by 150 km original scene, registering the image to a known set of coordinates, and removing the atmospheric component from the scene. Details of these steps are provided in Appendix 3.

Image processing

The primary reason for using multi-spectral remote sensing data in this project was to exploit the information beyond the visible spectrum. Instead of using a single image (the aerial photograph) to interpret geomorphic units, the multi-spectral and digital nature of Landsat allows production of many images from multiple band combinations. These images are created both from combinations of the original six Landsat bands and from indices and principle component analyses made possible by the digital nature of the data. The digital format also allows for contrast adjustments in the image that accentuate color differences.

The first step in this study was to produce imagery that displays the greatest variation between pixels. These images guide sampling in the field as they a) identify areas that are the same, enabling field personnel to streamline their sampling, b) identify different regions that must be sampled, and c) show contacts between regions of different materials. Three specific techniques were used in producing the images. First, commonly used, standard remote sensing band combinations were created. Second, the optimum index factor was calculated for each three-band combination of the original six Landsat bands to identify the combination that displayed the most variation for this specific scene. Third, standard indices and principle component analyses were performed. These procedures and indices can be calculated for any scene. After collection of field data, additional indices were calculated for this specific scene.

Standard band combinations
Several three-band combinations of the six Landsat Thematic Mapper (TM) reflectance bands have become standards in the remote sensing community. Table 2 presents three of these standard band combinations.

[1] A Landsat *scene* is the area covered by the Landsat data acquired by the satellite and provided as a data file. See Appendix 1 for more information about the scenes obtained for this study.

First, the 321 band combination is used to approximate a color aerial photograph as this combination uses only the visible bands. This combination is referred to as a "true" color image (Figure 7).

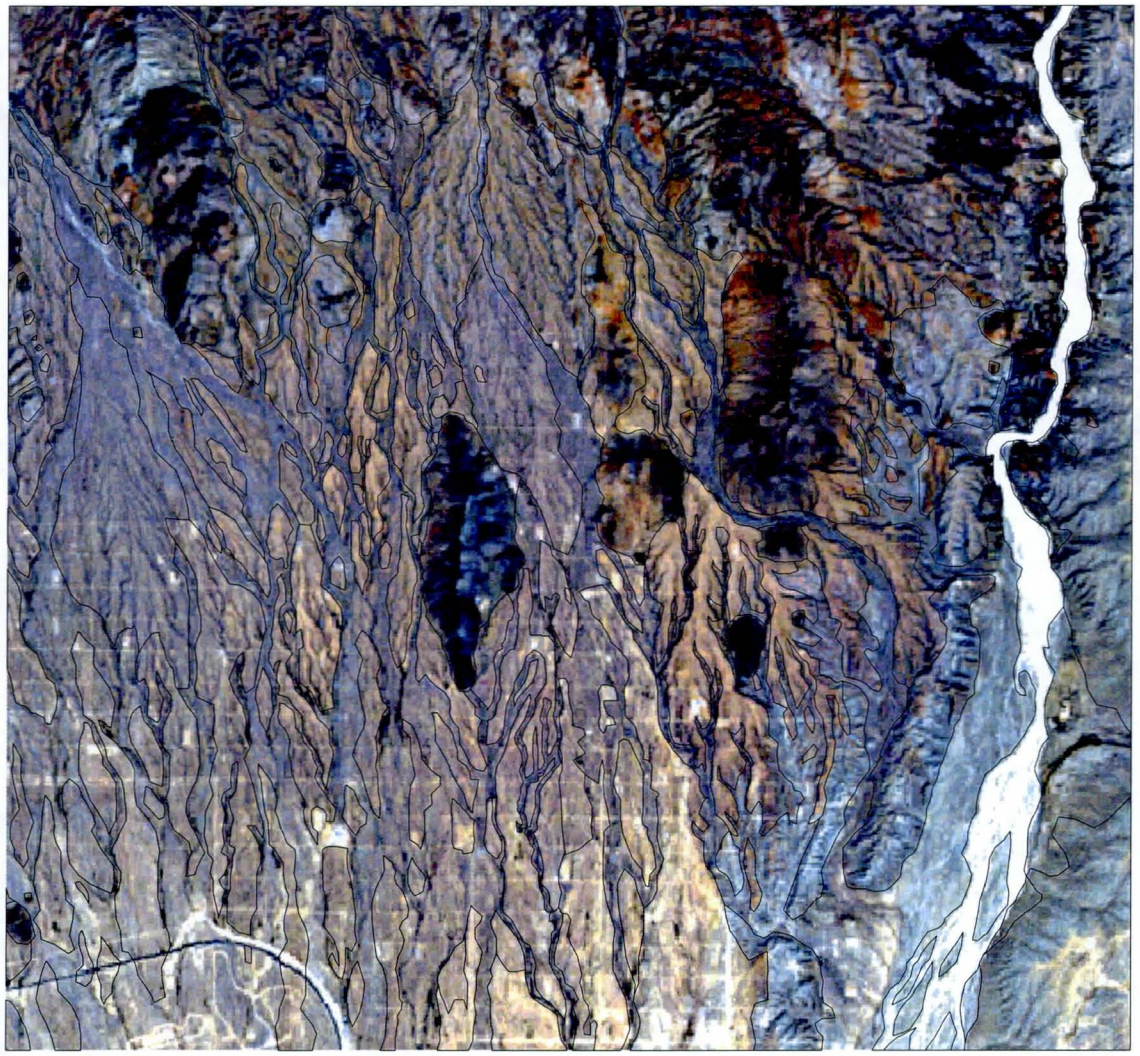

Black lines are unit boundaries shown in Figure 5.

6000 0 6000 12000 Feet

N

Figure 7. 321 (Visible) Band Combination Image

Second, a 432 band combination is commonly used to highlight vegetation. In a 432 band combination, vegetation appears in red due to the high reflectance of chlorophyll in TM Band 4. The red linear features in Figure 8 represent piedmont channels lined by dense riparian vegetation.

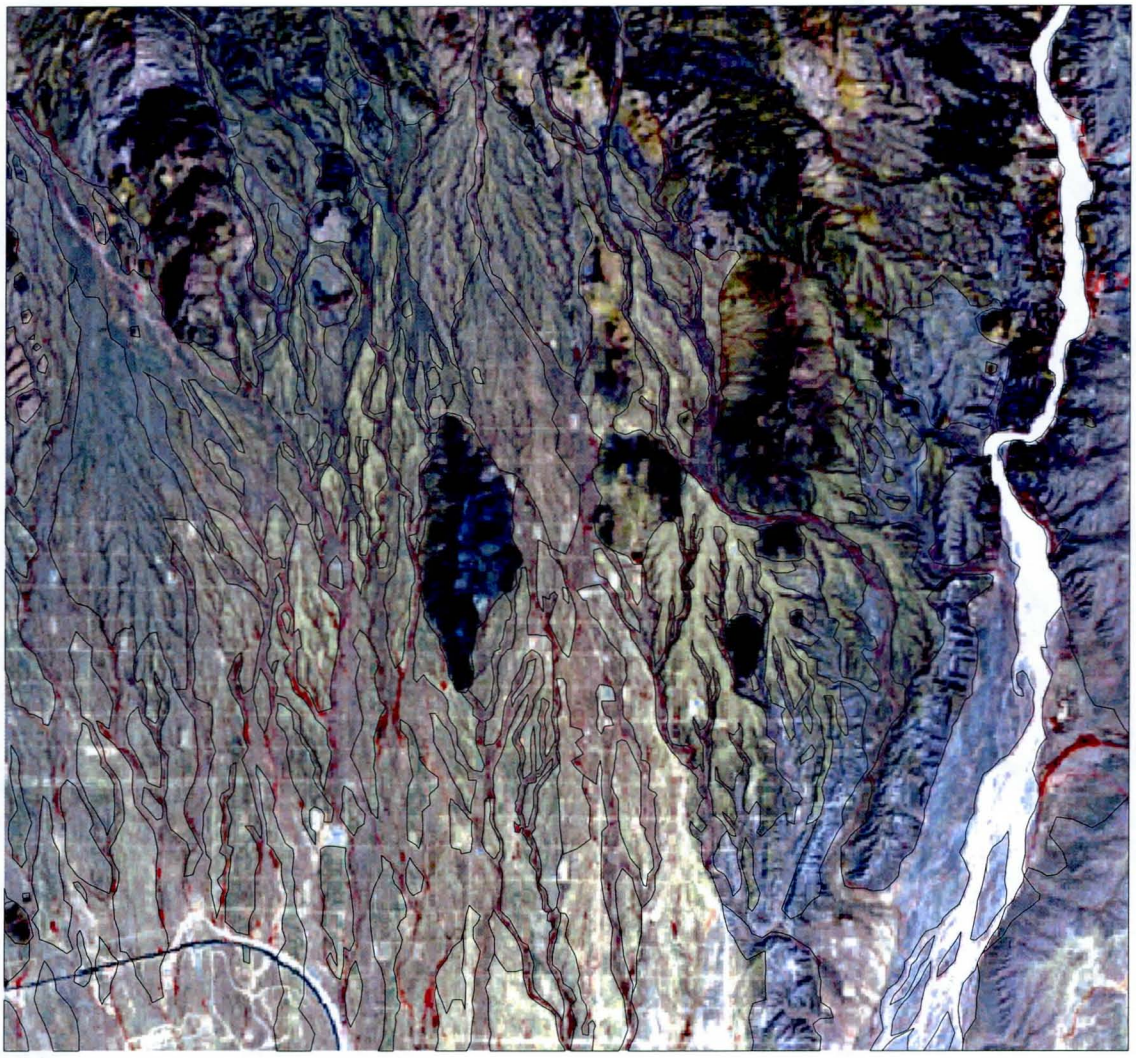

Black lines are unit boundaries shown in Figure 5.

6000 0 6000 12000 Feet

N

Figure 8. 432 Band Combination Image

Finally, a 742 band combination is often used in arid and semi-arid regions to detect compositional differences at the surface. In Figure 9, differences in bedrock types can be seen in the hills in the upper portion of the image. Similarly, the Hassayampa River terraces in the right portion of the image have a distinctive bluish "color" compared to the pinkish floodplain areas. The riparian vegetation shown as red in Figure 8 appears green in the 742 image.

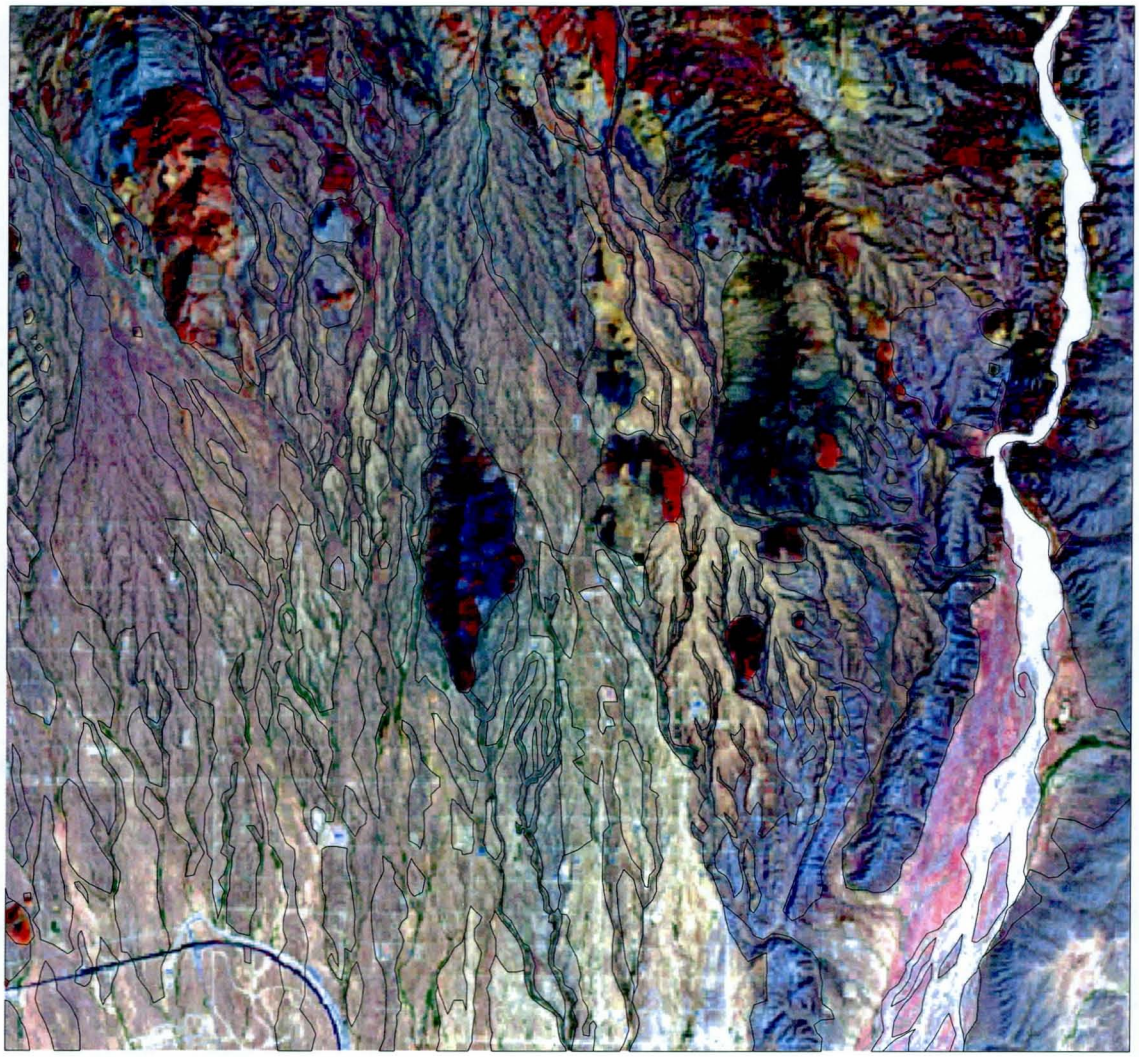

Black lines are unit boundaries shown in Figure 5.

6000 0 6000 12000 Feet

N

Figure 9. 742 Band Combination Image

As pixels in adjacent bands tend to be very similar, by choosing non-adjacent bands, more spectral diversity is displayed (Sabins, 1997) (See Table 2).

Table 2. Standard Band Combinations

	Band Combinations		
	321	432	742
Hassayampa River Channel	White	White	White
Piedmont channels	Black	Red to black	Black
Holocene units	Gray	gray to reddish pink and bright white	tan to red
Pleistocene units	Yellow, Brown	Pale yellow, green	Tan to greenish-gray
General Contrast Comments	Generally the units vary from gray to tan with little contrast difference	The active channels are clearly distinguished with their vegetation abundance. There is not much contrast between the Holocene and Pleistocene units.	Differentiation among the Pleistocene units (older being tan and younger being greenish-gray) and better differentiation between the Holocene and Pleistocene units.

Optimum Index Factor

The band combinations containing the greatest variation in a specific scene can be determined by calculating the Optimum Index Factor (OIF). The OIF uses the standard deviation of each band and the correlation coefficients between bands to derive an index that compares the amount of variation displayed in three-band red-green-blue (RGB) combinations (Jensen, 1996). The correlation coefficient is a dimensionless value that measures the interrelation between bands. Standard deviation and correlation coefficient statistics can be calculated by any of the standard remote sensing software programs. The largest OIF value defines the optimum band combination for a specific scene. The band combinations with the highest OIF values for this scene are given in Table 3.

As this project focused on the Quaternary units and not bedrock identification, OIF values were calculated for the entire study area image and an image with the bedrock areas removed. While the OIF values for these two images are not the same and do not have the same internal rankings, the five combinations with the highest OIF values are the same for both images. Notice that the OIF values are slightly less for the image with bedrock removed. This is a result of removing some of the variation in the scene by removing the bedrock. Also notice that the band combinations with the greatest amount of variation include bands beyond the visible spectrum (specifically TM bands 5 and 7). A 321 band combination, using information only in the visible, has an OIF in the lower third of the rankings demonstrating that much variation in the scene occurs beyond the visible spectrum and that information is lost by using only "true color" images equivalent to aerial photographs.

Table 3. Optimum Index Factor Data and Calculations

Correlation Matrix for Image with Reflectance values between 0 and 1

	Band 1	Band 2	Band 3	Band 4	Band 5	Band 6
Band 1	1.000	0.958	0.904	0.867	0.829	0.813
Band 2	0.958	1.000	0.962	0.933	0.886	0.877
Band 3	0.904	0.962	1.000	0.964	0.911	0.914
Band 4	0.867	0.933	0.964	1.000	0.923	0.909
Band 5	0.829	0.886	0.911	0.923	1.000	0.979
Band 6	0.813	0.877	0.914	0.909	0.979	1.000

Standard Deviations

	Image with bedrock	Image with bedrock removed
Band 1	0.034	0.03
Band 2	0.046	0.041
Band 3	0.057	0.05
Band 4	0.04	0.033
Band 5	0.091	0.076
Band 6	0.091	0.08

$$OIF = \frac{\sum_{k=1}^{3} s_k}{\sum_{j=1}^{3} ABS(r_j)}$$

Sk = Standard Deviation for band k

rj = Absolute value of the correlation coefficient

Calculated OIF value for each combination

Band Combination	Image with bedrock	Image with bedrock removed
357	0.085	0.074
257	0.083	0.073
157	0.082	0.073
457	0.079	0.068
237	0.070	0.063
235	0.070	0.061
137	0.069	0.062
135	0.069	0.061
347	0.067	0.059
345	0.067	0.058
247	0.065	0.057
127	0.065	0.058
245	0.065	0.056
125	0.064	0.056
147	0.064	0.057
145	0.063	0.055
234	0.050	0.044
123	0.049	0.044
134	0.048	0.043
124	0.043	0.039

Cells in yellow are band combinations with highest OIFs compared to the visible (123).

Calculating standard indices

Because Landsat images are digital, with each pixel being represented by a number, indices can be created by performing mathematical operations on the pixels. The mathematical operations accentuate different aspects of the material spectra, specifically the convexity of spectral slopes and the presence of absorption features such as the dips seen in the fir tree spectra shown in Figure 3 near 1.5 and 2.0 microns. Most frequently, the pixels in one band are divided by the pixels in another resulting in a ratio. Ratios are useful because they emphasize color differences and spectral similarities without being affected by changes in illumination caused by slope, shading, etc. (Gillespie et al., 1984).

Indices calculated for this study included standard indices and indices developed specifically for this study area and project. Standard indices include a normalized difference vegetation index (NDVI), a soil adjusted vegetation index (SAVI), a clay/hydroxyl ratio, an opaques ratio and an

iron ratio. After the field data were collected, a second set of ratios were calculated based on the specific geomorphic unit spectra to develop images that better discriminated between these units. Appendix 7 provides figures and additional explanation of these standard indices.

Developing scene specific indices

Representative pixels were chosen from different geologic units identified in the field. Image spectra taken of these pixels showed two major trends (Figure 10). First, the shapes of the spectra are very similar, only the placement of the spectra is shifted along the y-axis. Second, the peak seen in TM band 3 varies from acute to almost flat. These spectral observations were used to develop two scene specific indices.

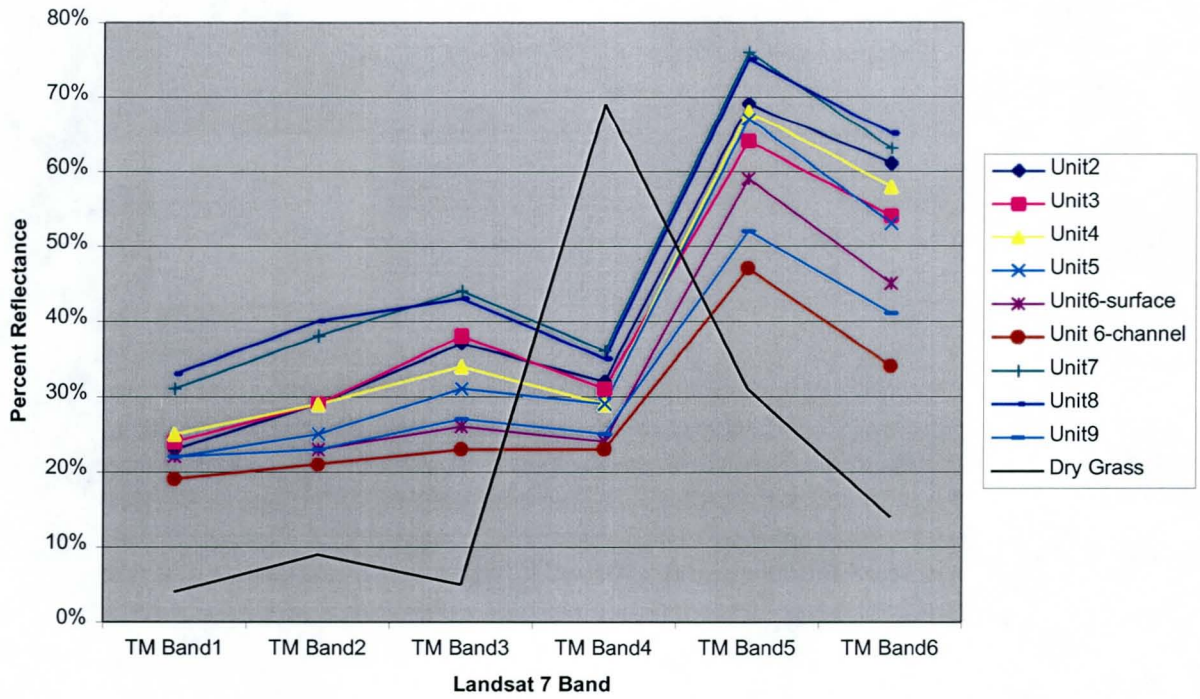

Figure 10. Representative Unit Spectra

The similarity in spectral shape is due to the fact that the surface materials on the same piedmont have a similar origin. A 30 m Landsat pixel of an alluvial fan deposit is a mixture of its clast compositions, vegetation, and any post-depositional changes (such as soil, pavement, varnish, caliche, etc.). For a given piedmont, the clast composition should be similar regardless of the age of the deposit since they generally have the same source areas. The type of vegetation is also similar, but typically only varies by one or two species and in the density of plant placement. The contribution to the spectra of post-depositional changes is relatively small. Thus, expecting drastic changes in the shape of the spectra due to small variations in pavement development, varnish thickness, or clay accumulation is unrealistic.

However, the shift along the y-axis indicates that a material property of these surfaces is changing the overall brightness of the pixels. The most likely causes for this variation are degree of pavement development and amount of vegetation. Brightness is decreased with increasing pavement development because the brighter, underlying smaller particles are covered by darker clasts. A decrease in vegetation will increase the brightness of a pixel because vegetation

typically darkens a surface. These two factors vary inversely with increased pavement development (which darkens a pixel) and decreased vegetation (which brightens a pixel).

The change in shape around TM Band 3, varying from a sharp peak to almost flat (Figure 10), is due to vegetation. Standard vegetation indices are based on the characteristic shape of vegetation with a sharp increase from TM Band 3 to TM Band 4. However, desert vegetation is typically widely spaced and does not have the standard deciduous leaf structure, making the standard spectral shape rare. Thus, while field data indicate that many of the pixels represented on this chart have vegetation, the spectra do not exhibit the classic vegetation shape as seen in the dry grass spectra (compare Figure 11 and 10).

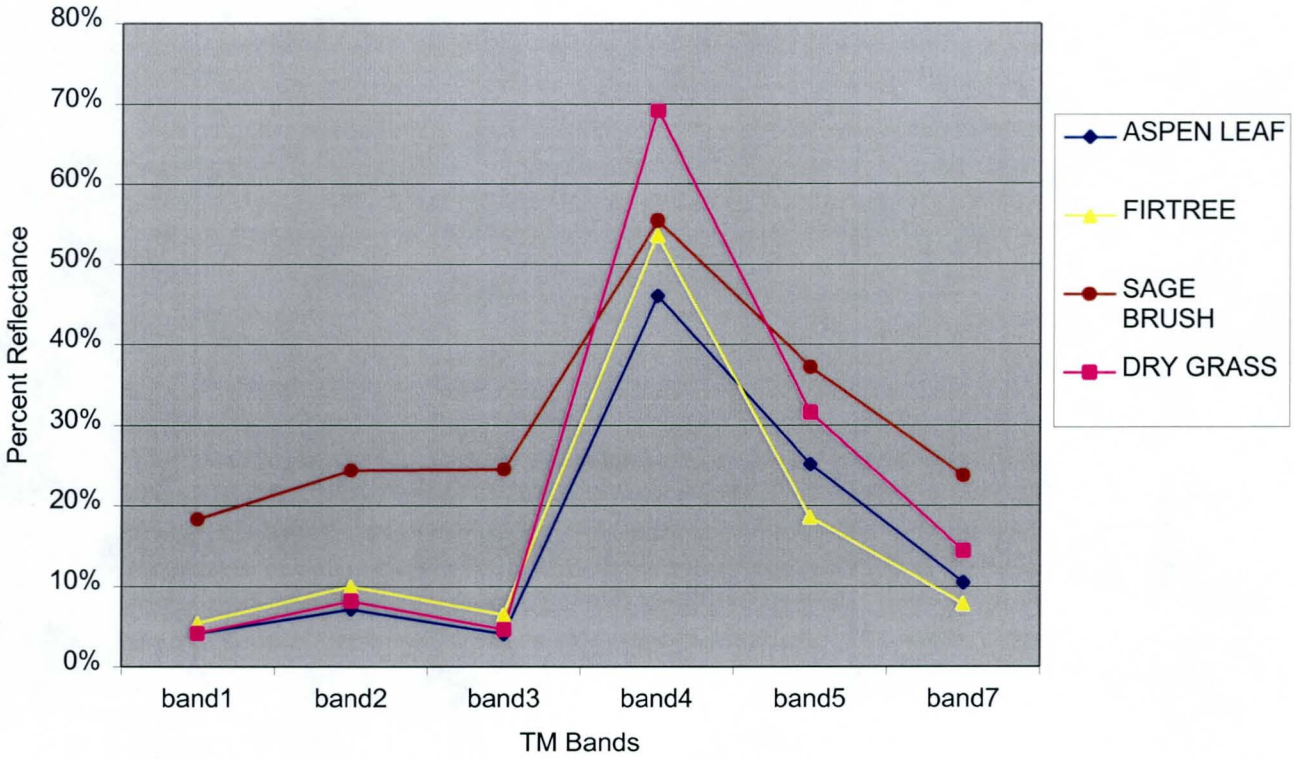

Figure 11. Lab Spectra of Vegetation Reduced to Landsat Resolution

However, if small percentages of the vegetation spectra were added to the spectra of Unit 2, the result would be a decrease in TM Band 3 and an increase in TM Band 4 as the vegetation spectra is lower in TM Band 3 and higher in TM Band 4 than Unit 2. Thus, the addition of vegetation to a Unit 2 Pleistocene piedmont spectra would result in a reduction of the peak at TM Band 3; surfaces with less vegetation have sharper peaks, while surfaces with more vegetation have flatter peaks. This relationship is confirmed from field data that document that Unit 2 and Unit 3 have the sharpest spectral peak at TM Band 3, have the least amount of vegetation, while Unit 6, having a relatively flat peak at TM Band 3, has denser vegetation (Figure 12).

Figure 12a. Photo of Unit 2

Figure 12b. Photo of Unit 6

Indices calculated specifically for this scene

Three scene specific indices were created to differentiate the geomorphic units in the study area based on the spectral observations made above (Figure 13). The SWIR 2 (short wave infrared index number 2) index accentuates the shift along the y-axis caused by increasing amounts of reflectance by multiplying TM Bands 3 through 6 (3x4x5x6). This results in higher index values for "bright" pixels such for the Hassaymapa River channel (Unit 8) and the overbank silty deposits (Unit 7), and lower values for darker areas. This over brightness is dependent on the amount of vegetation and degree of pavement development.

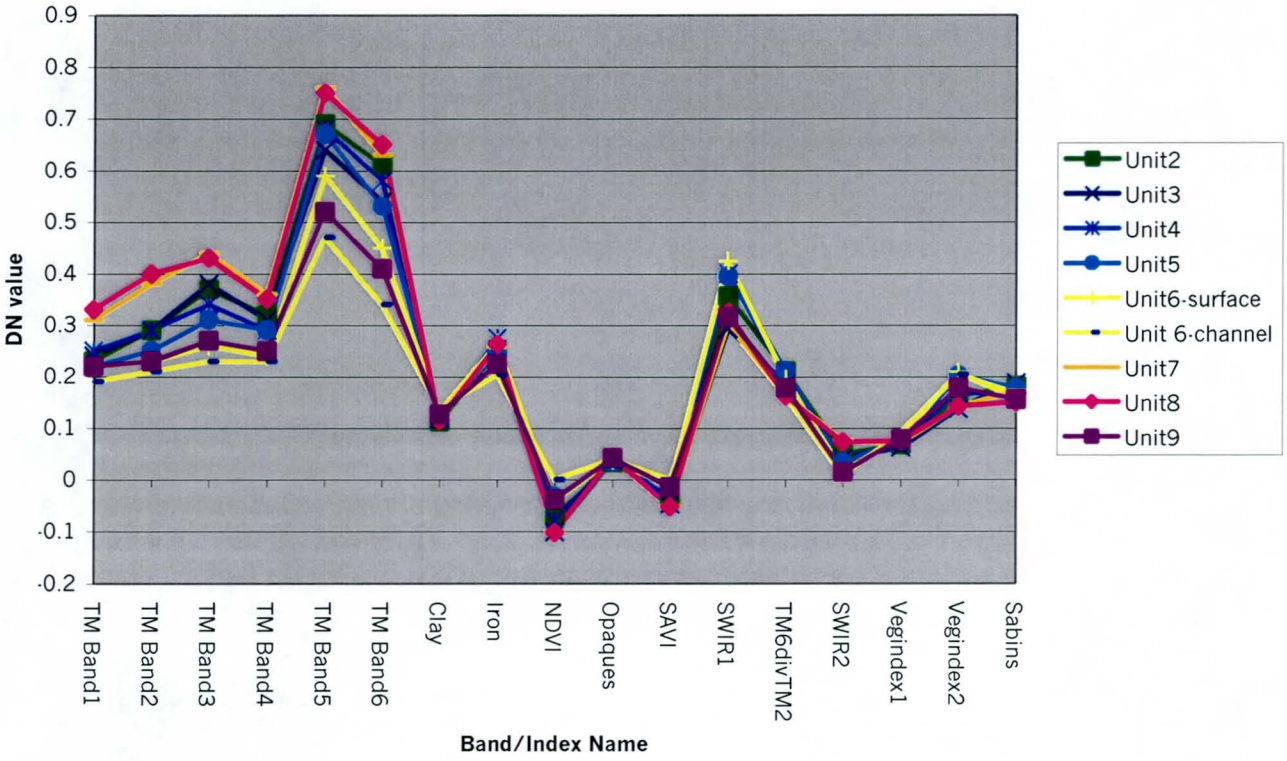

Figure 13. Representative Pixels from Geologic Units

Two vegetation indices, Vegindex1 and Vegindex2, were developed. Vegindex1 is an index of the convexity observed at TM Band3 (see Figures 10 and 13). Spectra with higher index values have flatter peaks and are associated with more vegetation. Spectra with lower index values indicate sharper peaks and sparser vegetation. Vegindex2 multiples the values of two vegetation indices: one based on the classic vegetation spectra and the other based on change due to the consideration of desert vegetation characteristics in this study. TM Band 4 divided by TM Band 3 is often used as a vegetation index based on the high reflectance of vegetation in TM Band 4 as discussed above. Multiplying the 4/3 ratio by TM Band 5 divided by TM Band 3 accentuates the flattening of the peak at TM Band 3. Vegindex2 produces large values for pixels with vegetation and lower values for pixels with sparse vegetation.

Map generation

The geomorphic map was created by on-screen digitization using multiple band combinations (Figure 5). The band combinations included the original bands, standard indices, and scene-specific indices to accentuate the spectral differences of each unit. While many combinations were used during the process, the two most useful combinations in this study proved to be the 357 band combination and the SWIR2-Vegindex1-TM5 combination.

The 357 band combination had the highest Optimum Index Factor (OIF) and showed the most variation between the late Pleistocene and Holocene units. In this band combination, Holocene units are green due to the denser vegetation, causing higher reflectance values in TM Band 5. The Pleistocene units, characterized by sparse vegetation, are displayed in red, with the darker red indicating older mid-early Pleistocene units and the grayish-pinks showing younger late Pleistocene units (Figure 14).

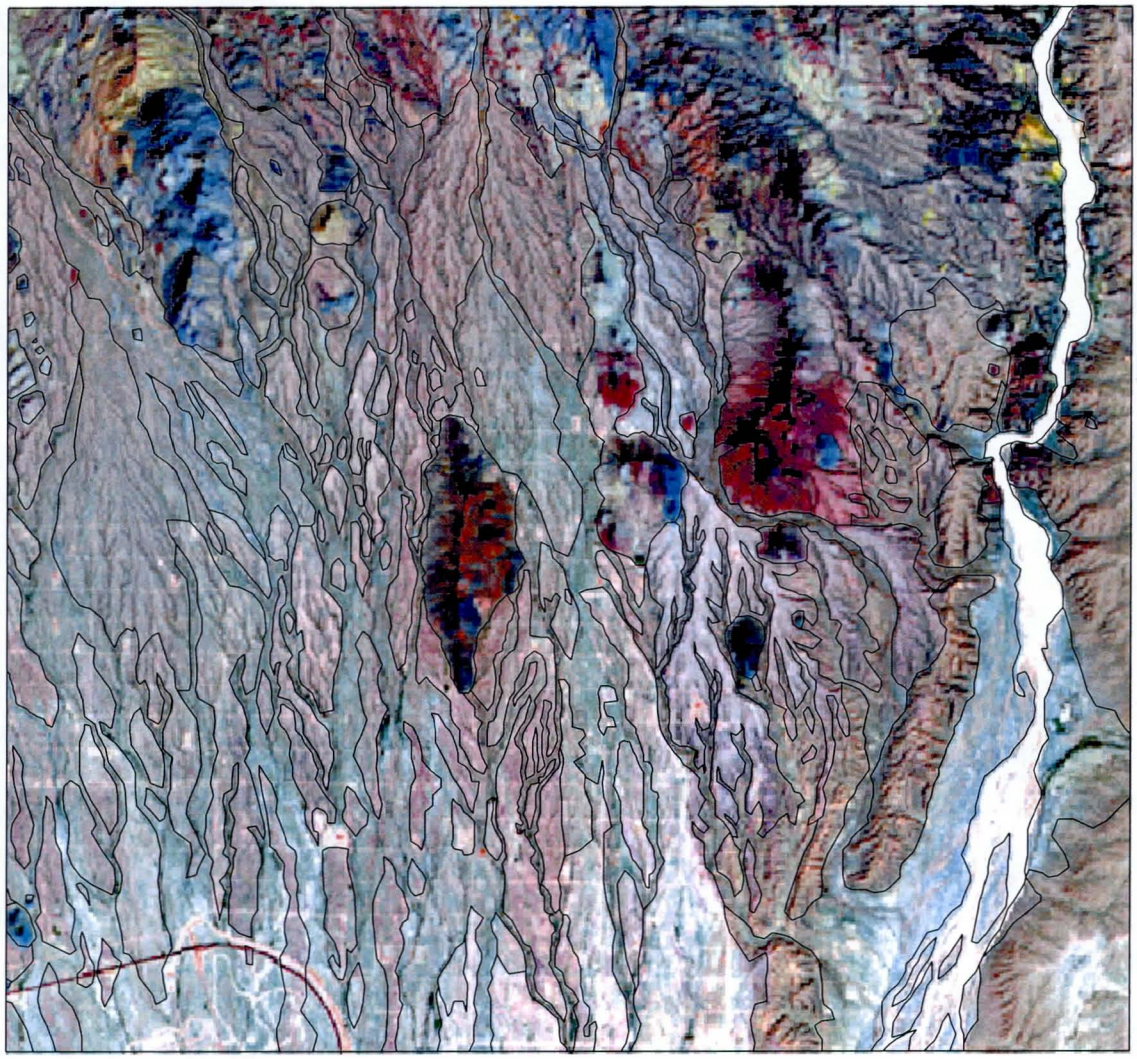

Black lines are unit boundaries shown in Figure 5.

6000 0 6000 12000 Feet

N

Figure 14. 357 Band Combination Image

The SWIR2-Vegindex1-TM5 combination used two scene specific indices and an original TM band. The surfaces display along a magenta to green continuum. Early to mid-Pleistocene deposits (Units 2 and 3) are seen in bright magenta and deep purple. Younger Pleistocene units (Units 4 and 5) are displayed in lighter purples and mixtures of lavender and green. Holocene deposits (Unit 6) are displayed in green. The exception to this is Unit 7 (Holocene overbank and sheetflood deposits), while Holocene in age, displays in magenta, similar the oldest Pleistocene unit. This is due to the similarity between the Unit 7 and Unit 2 characteristics measured by the indices used in this combination; both have sparse vegetation and are both bright (Figure 15).

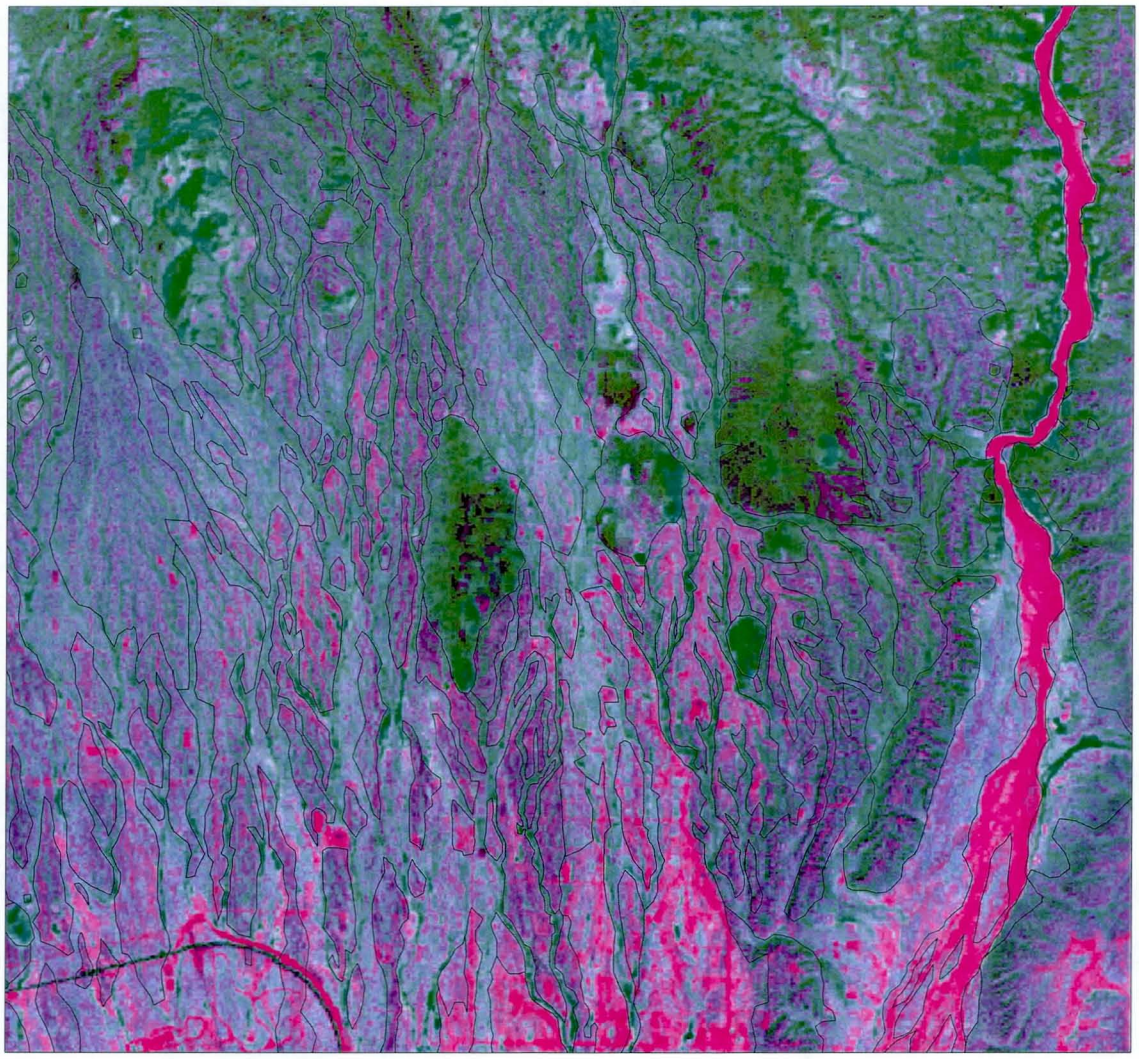

Black lines are unit boundaries shown in Figure 5.

6000 0 6000 12000 Feet

N

Figure 15. SWIR2-Vegindex1-TM Band 5 Combination Image

Expert systems classification

Creating the geomorphic map through on-screen digitization from multiple remote sensing band combinations is a very similar process to traditional mapping from aerial photographs. The geologist groups similar regions together and draws bounding lines between these regions. By using multi-spectral datasets with more spectral information than aerial photographs, a first-order, automated process to delineate these geomorphic units based on their spectral characteristics was attempted. However, due to the complexity of alluvial fan geomorphology and subtle differences between adjacent surfaces, the study was unable to generate automated maps with the same level of unit detail as the on-screen digitized geomorphic map. However, we

were able to develop an automated process that differentiates broad classes of geomorphic units. In other words, while the expert classification system could not consistently differentiate older Pleistocene deposits with well-developed pavement from younger Pleistocene deposits with moderately well-developed pavement, it could differentiate the Pleistocene deposits from the Holocene deposits. Differentiation of Holocene and Pleistocene surfaces is generally sufficient for the delineation of flood and erosion hazards.

To develop the expert systems classification for this study area, the vector geologic map (Figure 5) was used to generate statistics for each of the geologic units. Mean, maximum, minimum, and standard deviation of the original TM bands and indices were calculated for each of the nine geologic units which produced a mean spectra for each of the geologic units. The mean spectra for each unit were plotted with error bars of one standard deviation (Figure 16). However, the geologic units in the study area are heterogeneous. Polygons defining regions assigned to Unit 2 may include areas with poorly developed pavement due to localized bioturbation or small drainage networks. Despite the difference in their surface expressions, both areas are part of the same geologic deposit and thus the same geologic unit. The heterogeneity affects the calculated statistical parameters. Therefore, a single representative pixel was also taken from each unit and plotted in a companion graph (Figures 13 and 16). Figure 16 shows the statistical variation as the black "error" bars while the mean spectra is represented by the colored line for each unit.

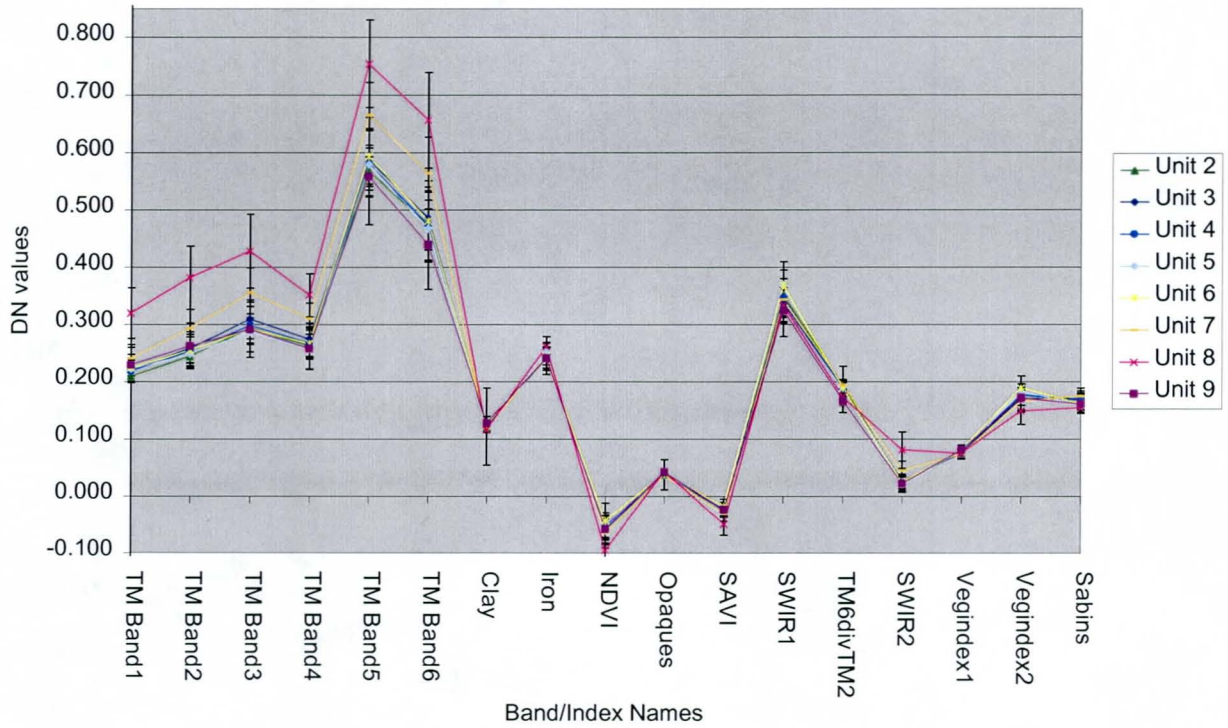

Figure 16. Spectra of geologic units

This data showed that the Pleistocene units were very similar in all the bands – that is, each of the Pleistocene unit mean spectra plotted within the error of the other Pleistocene unit's statistics. However, the Pleistocene units as a group could be differentiated from the Holocene units. Therefore, the decision was made to use the expert classifier not to produce a geologic map, but instead to group the geologic units into flood hazard units based their frequency of inundation by channel or overbank flow. Correlating flood prone characteristics to these geomorphic units

relies on several assumptions based on the current understanding of piedmont geomorphic processes and the relationship between geology and vegetation. These assumptions are as follows:

1. Any surface with desert pavement has not been actively flooded for at least 10,000 years.

2. Moderately vegetated piedmont surfaces have experienced flooding in the last 10,000 years. According to McAullife (1994) there is a progression of vegetation communities on piedmont surfaces that is heavily influenced by the subsurface geomorphology, particularly that of a clay horizon. As pavement develops the density of plants is reduced because the pavement impedes plant growth and propagation.

3. Densely vegetated piedmont channels and large, bright, un-vegetated channels, while ephemeral, are frequently inundated. Smaller channels draining the piedmont typically contain dense vegetation. The channels themselves, however, may be too small to occupy an entire 30 m pixel. As channels increase in size they become bright and detectable at a 30 m pixel grid. The Hassayampa River channel is an example of this larger, active channel.

The resulting three units from the expert classification system were: 1) a frequently inundated unit, 2) a not-frequently inundated unit, and 3) a bedrock unit. The frequently inundated category included piedmont channels, over-bank silt deposits, and the Hassayampa River channel (Units 6, 7, and 8). The infrequently inundated category included all the Pleistocene piedmont deposits and the Hassayampa River terraces (Units 2, 3, 4 and 9). The early Holocene unit (Unit 5) has characteristics of both an active surface and inactive surface as it has an incipient clast lag developing, but also a dense vegetation community characteristic of younger, more active surfaces. This unit was not consistently classified as either frequently or infrequently inundated, but instead pixels representative of this unit are found in both flood prone area classifications.

This expert system was not based on grouping polygons with geologic characteristics into flood groups, but instead on the remote sensing characteristics of these units to group individual pixels. The statistical data for the polygons of the geologic map and the mean and representative pixel spectral plots were examined. Three indices were found to consistently differentiate the Pleistocene and Holocene units: SWIR2, Vegindex2 and Sabins (Figure 17). Vegindex2 (5/3x4/3) differentiated the sparsely vegetated Pleistocene (Units 2,3,4) surfaces from the more densely vegetated Holocene surfaces (Unit 6), with the Pleistocene surfaces having values less than 0.18. However, the overbank silt deposits (Unit 7) and the Hassayampa River channel (Unit 8) are also characterized by Vegindex2 values less than 0.18 due to their sparse vegetation. These units can be differentiated from the Pleistocene units by their high SWIR2 (3x4x5x6) index values caused by their high reflectance values in all bands, resulting in a "bright" appearance. Included in Unit 6 are low flow areas of the Hassayampa River which are also not highly vegetated, but are not as bright as the main channel. These regions have a high Sabins index value (5/7x3/1) reflecting their low clay and iron contents, to be expected in active regions.

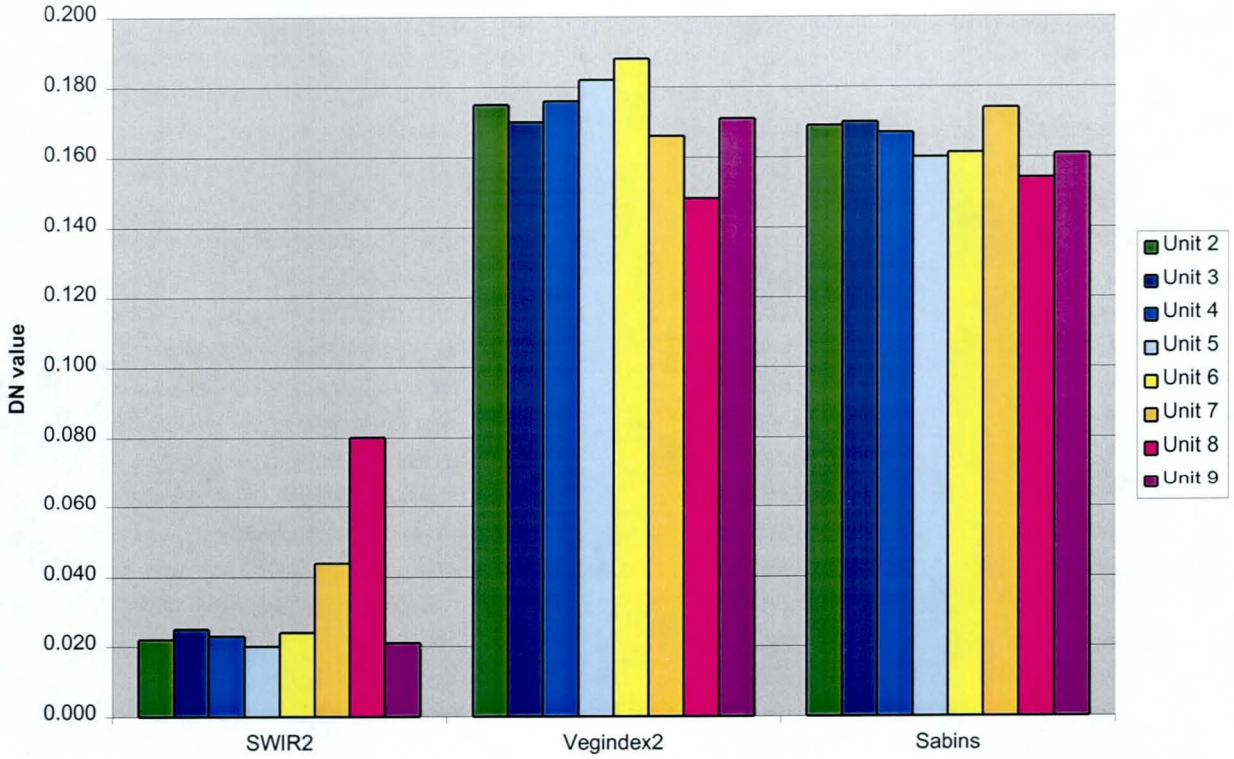

Figure 17. Mean Spectra Used to Establish Expert Classification

Therefore, the following decision rules were used for the expert classification system:

Frequently inundated

1. Moderately vegetated piedmont surfaces and densely vegetated piedmont channels (Units 5 and 6)
2. Very bright, unvegetated silty deposits (Unit 7)
3. Very Bright, unvegetated larger channels (Unit 8)
4. Moderately bright, unvegetated low flow areas associated with larger channels (Unit 6)

Infrequently inundated

1. Sparsely vegetated surfaces with some degree of pavement development (Units 2, 3, 4, and 5)

Figure 6 presented earlier shows the results of the expert classification for the study area.

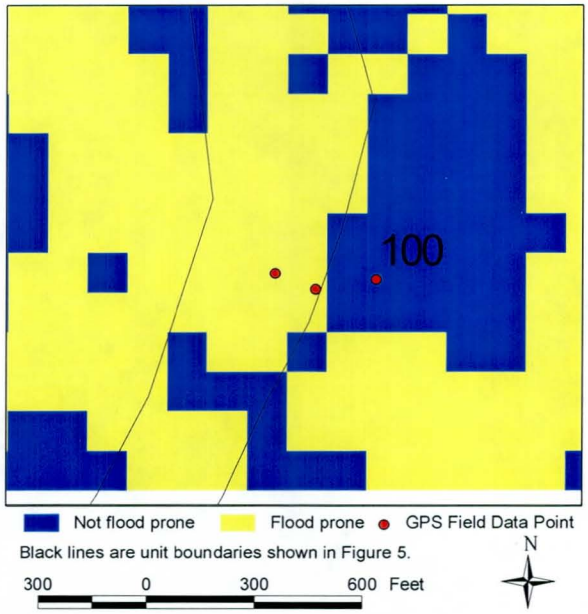

Figure 18. Close up of the Expert Classifier Map

When overlaying the vectors of the geologic map on top of the raster output of the expert systems classification, heterogeneity within units can be seen (see Figure 6). This is consistent with the heterogeneity discussed above inherent in alluvial fan units. For example, Figure 18 shows an enlargement of an area of the expert classifier map (Figure 6) with points indicating sites where field data was taken. Point 100 represents a small patch of well-developed pavement surrounded by a broader expanse of silty over-bank deposits. The expert classifier identified these small regions on a pixel by pixel scale that is unfeasible in traditional geologic mapping, which is based on grouping areas into units.

Overall, the general correspondence of the mostly blue areas with the Pleistocene units and the mostly yellow areas with the late Holocene units can been seen.

PART THREE: Discussion – Lessons Learned

The results of the remote sensing based geomorphic and flood prone area map production indicated that Landsat data could be used to differentiate Pleistocene and Holocene surfaces in the Jackrabbit Wash watershed. Some of the limitations and a comparison of the remote sensing-based results with traditional methods is presented in Part Three.

Limitations of the study technique

There are several inherent limitations in available Landsat data that handicap its use in the delineation of flood prone areas at the level of detail required by FCDMC for regulatory purposes. The limitations include image/sensor resolution, spectral combination, and registration of data.

First, the approximately 30 m by 30 m pixel size provided by Landsat sensors does not allow for the spatial precision required of floodplain delineation. As an example: a small wash may have only a very narrow channel and adjacent floodplain, perhaps 15 meters (49 feet) wide. This floodplain would be lost in the 30 m pixel of the Landsat image. The large pixel size also produces a stair-stepped or pixelated delineation.

Second, pixel size also causes a spectral combination problem. For example, a Landsat pixel comprised of 20% flood prone area and 80% non-inundated Pleistocene terrace would have a spectral signatures that more closely resembles the terrace than the floodplain, and the pixel might be classified as non-inundated terrace ignoring the small channel.

Third, map registration is challenging because the raw Landsat scene is not tied to geographic control points. The potential exists for errors to occur in the placement of the scene when tying a 30-meter pixel to more precise (i.e. sub-meter to centimeter level) control points such as those used in floodplain mapping.

Fourth, Landsat data are also limited to the detection of surface characteristics. Valuable information about the subsurface such as the degree of soil horizon development and caliche development is not detectable by the Landsat sensors. Surface vegetation was used as a proxy for subsurface conditions in the current study.

Fifth, remote sensing techniques require specialized image processing software, such as ERDAS Imagine. The use of the software also requires trained personnel able to operate the programs.

Finally, the approach used in this study relies heavily on the assumption that surfaces flooded in the geologically recent past are likely to be flooded in the future and visa versa. This assumption can be violated on rapidly aggrading alluvial fans or on recently incised arroyo systems.

Required skill set

The required skill set needed to produce this report is larger than the skill set needed to implement it. Several skills and/or knowledge sets are needed to complete the analysis of remote sensing data for floodplain delineation. These include:

- Software operation (Imagine (or other image processing software), GIS)
- Remote sensing techniques (band ratios, index generation, etc.)
- Knowledge of geology/geomorphology (groundtruthing, influences of parent material, and fluvial processes)
- Familiarity with FEMA guidelines for floodplain mapping
- Understanding of hydrology and open channel hydraulics

To conduct a study using the techniques described in this study one would need to have a familiarity with image processing software and Geographic Information Systems (GIS). ERDAS Imagine image processing software was used in this study. Additionally, it would be helpful to possess knowledge of what the different bands represent in the Landsat scene, the utilization of common band ratios, and index computation analysis is useful in the compilation of the expert classification. A general knowledge of statistics would also be helpful. Since the work of compiling the expert classification has been completed with this project, the most useful skills would be a working knowledge of ERDAS Imagine so that the specific steps could be followed to produce a final image. These steps are detailed in the appendices of this study.

Interpretation of the geologic information presented through the remote sensing data required knowledge of geology and geomorphology. The use of the technique developed in this study in other areas will require some knowledge of the local geology and geomorphology. Differences in geology will result in differences in the spectra reflected by the surface. These differences will result in different values for pixels, so that threshold values for identifying flood prone areas for the expert classification system will likely be different.

Finally, a general familiarity with Federal Emergency Management Agency (FEMA) guidelines for floodplain mapping, and traditional hydrology and hydraulic approaches would help provide valuable context for the results of a similar study.

Comparison of remote sensing results with traditional methods

In order to provide a context for the remote sensing results, a comparison of the expert classification image with traditional approximate floodplain delineation results was made. The floodplain delineated in the draft *Approximate Zone A Floodplain Delineation Study of Watershed 00, FCD 2000-C019* (JEF, in progress) serves as a point of comparison for this study. The Watershed 00 floodplain lines used in this study are preliminary, subject to District and FEMA approval but are unlikely to change significantly at the scale shown in Figure 19. Figure 19 shows these preliminary approximate 100-year floodplains plotted over the expert classification flood prone area image.

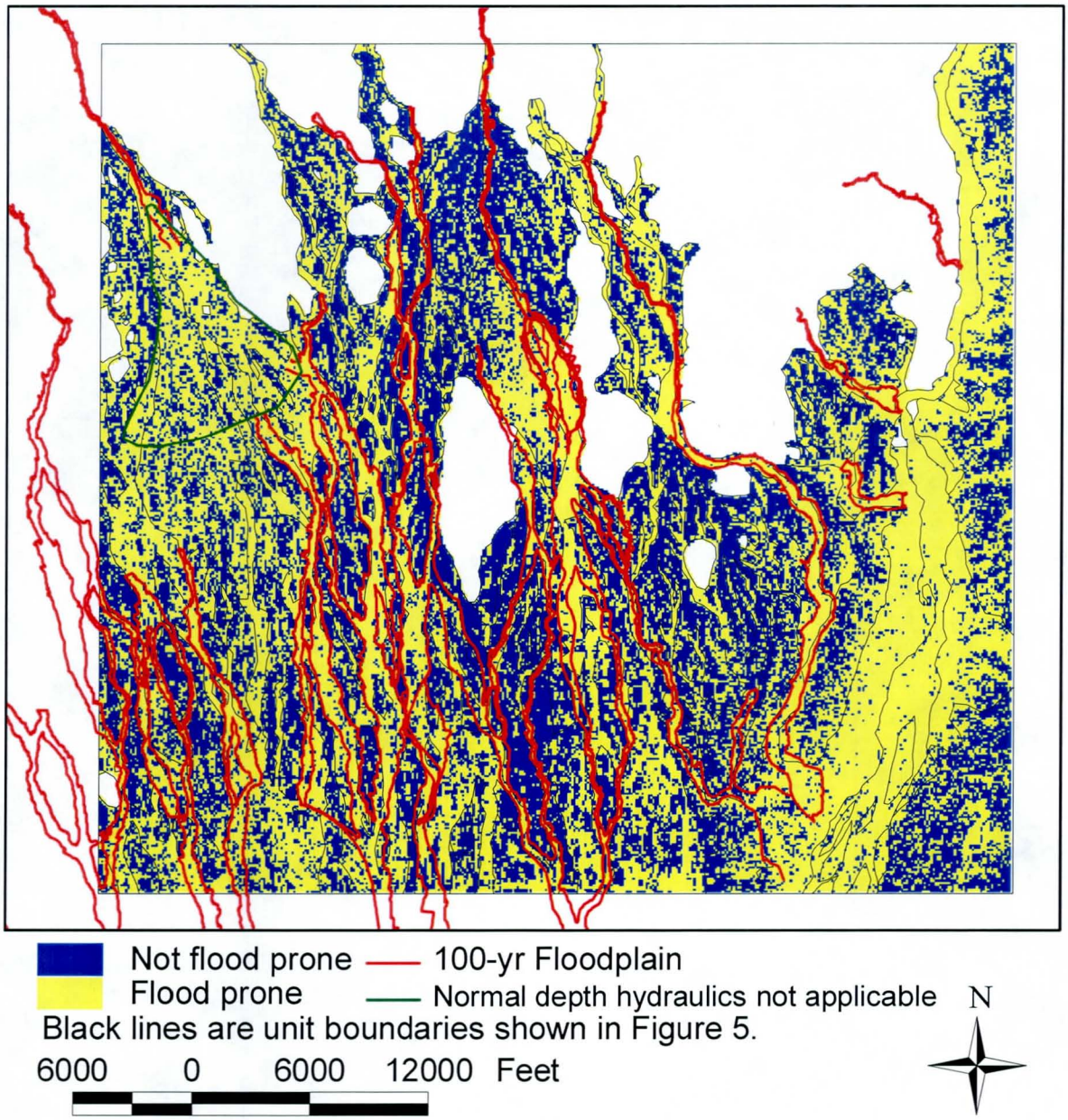

Figure 19. Comparison of Expert Classification and Approximate FDS Floodplain

Spatial comparison

Comparison of floodplain delineations from the traditional methods and the binary flood-prone/non-flood-prone map created by the remote sensing techniques indicates that differences between the two are substantial. In some instances, the expert classification showed inundation where the traditional approximate hydraulic methods do not. In other cases, the traditional approach shows a floodplain in an area classified as not flood prone by the expert remote sensing system. Figures 20-24 show examples of various manifestations of the differences between the two approaches. The figures show screened-back overlays of the flood prone area map over the aerial

photograph with the preliminary 100-year floodplain delineations. Again, blue denotes not flood prone and yellow denotes flood prone as determined by the expert systems classifier. Note that the scale of each figure is slightly different. Again, the pixel size of the yellow and blue squares is about 100 feet on a side.

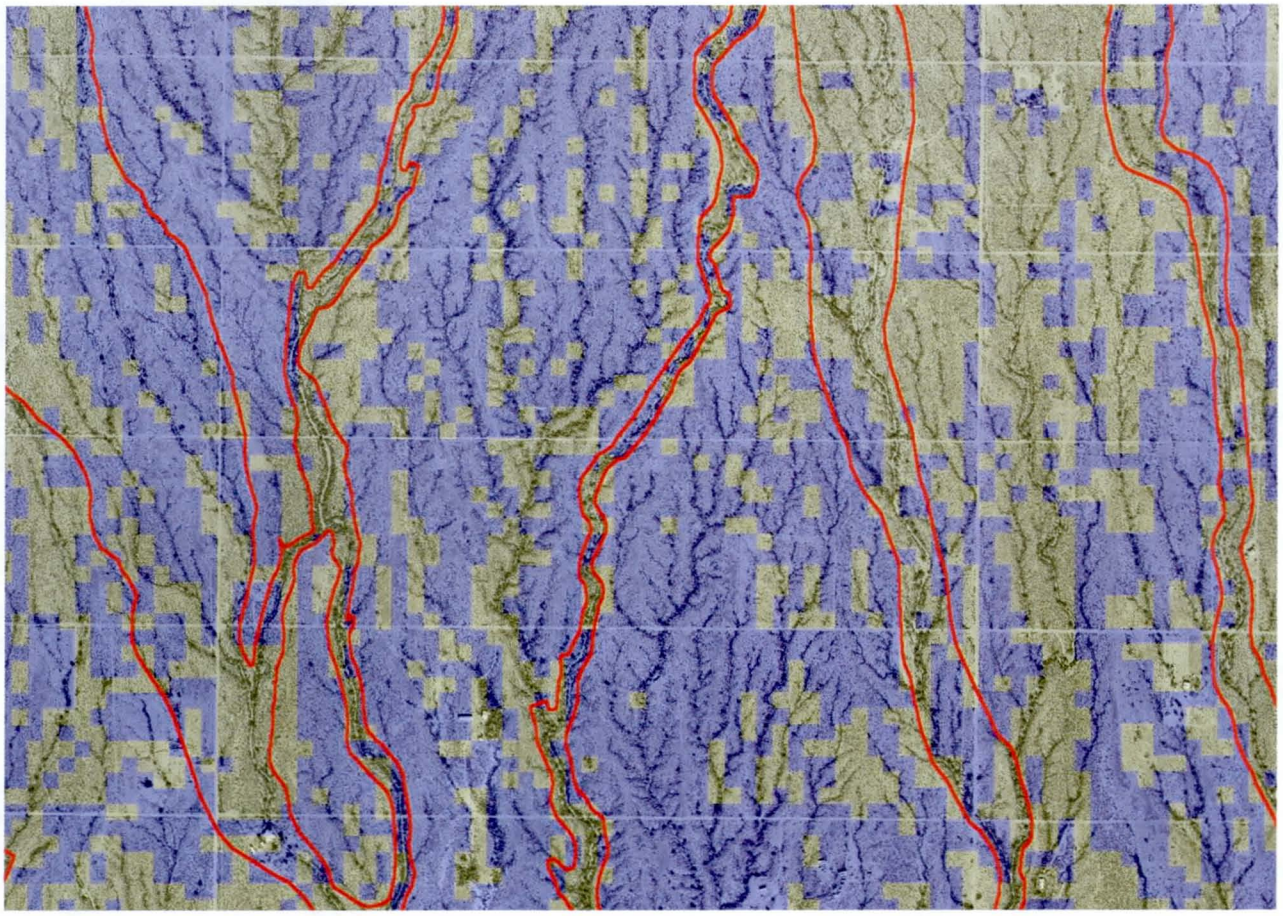

Figure 20

Figure 20 shows a narrow channel near the middle of the figure that is partially missed by the expert system classifier. A non-continuous series of yellow pixels approximates the alignment of the wash. The size of the wash may be responsible for the discontinuous depiction. Figure 20 also shows a broad area in the right half of the figure that is classified as flood prone by the expert system, but not delineated as 100-year floodplain in the *Approximate FDS*. However, the aerial photograph shows numerous small channels that originate locally in this vicinity. Other areas throughout the figure show small, local channels that are variously classified flood prone or not flood prone.

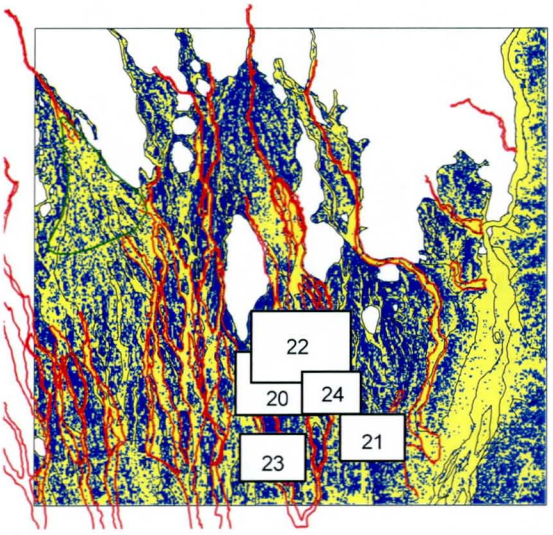

Index Map

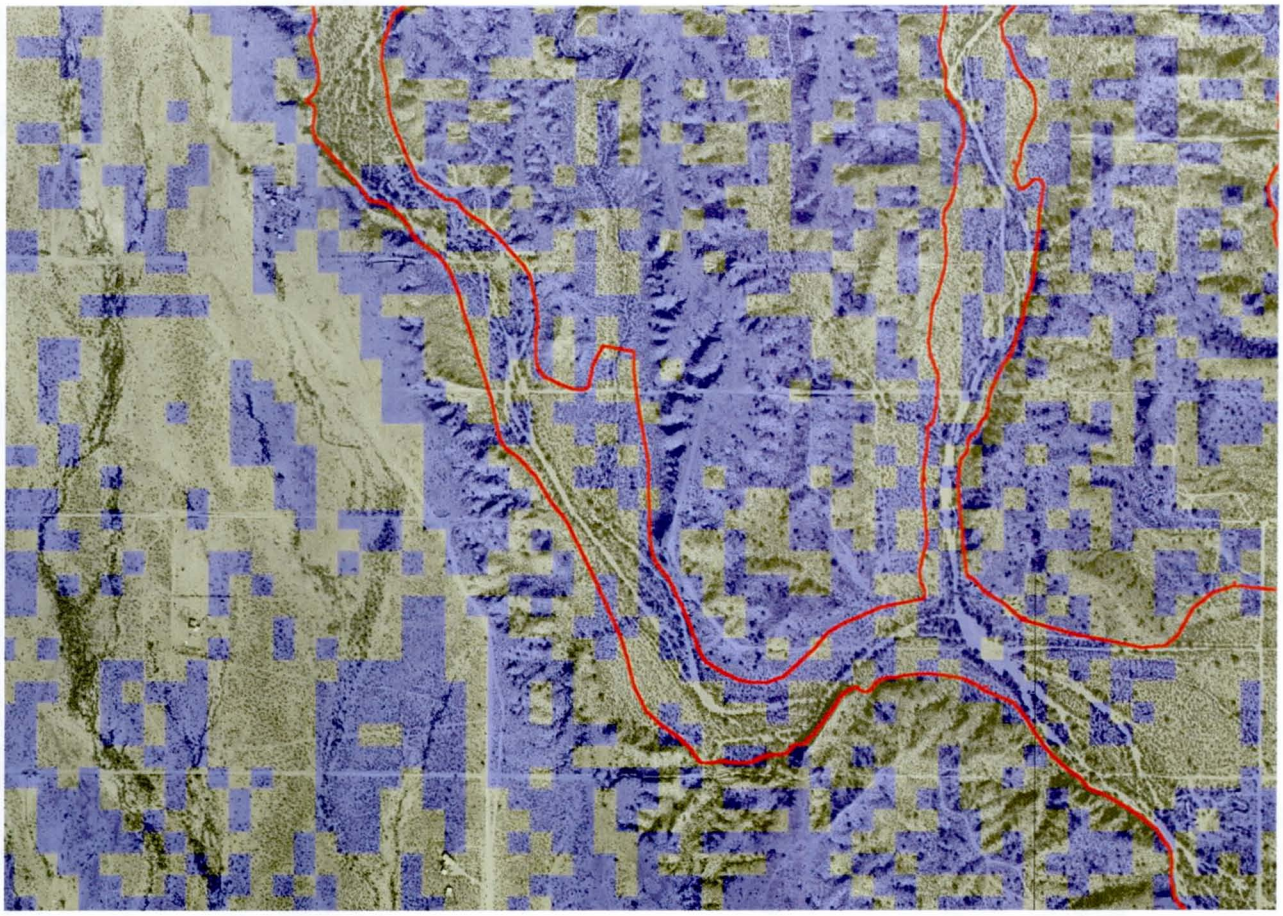

Figure 21

Figure 21 shows a wash and its tributary that contribute directly to the Hassayamapa River. They flow through a deeply dissected area of old geomorphic surfaces. .Again, much of the obvious channel area identified as 100-year floodplain in the *Approximate FDS* is correctly classified, while other areas are not. In particular, a large area in the left third of the figure is classified as floodprone. One large obvious shallow wash occupies the far left portion of the figure. Additional smaller wases are also present in this area. The heavily dissected areas between the two red floodplains show up as a checkerboard of blue and yellow with a slightly higher proportion of blue.

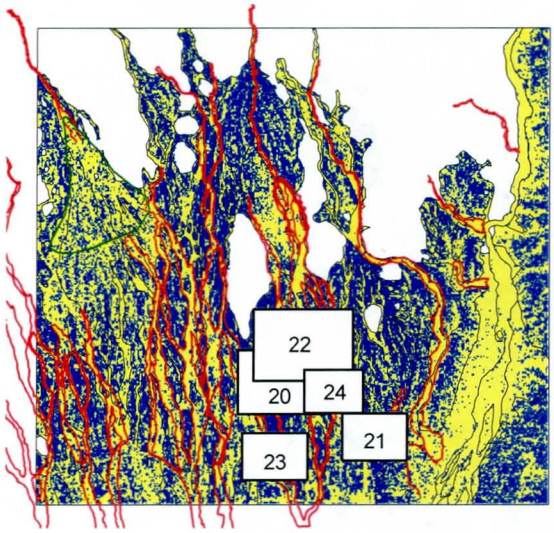

Index Map

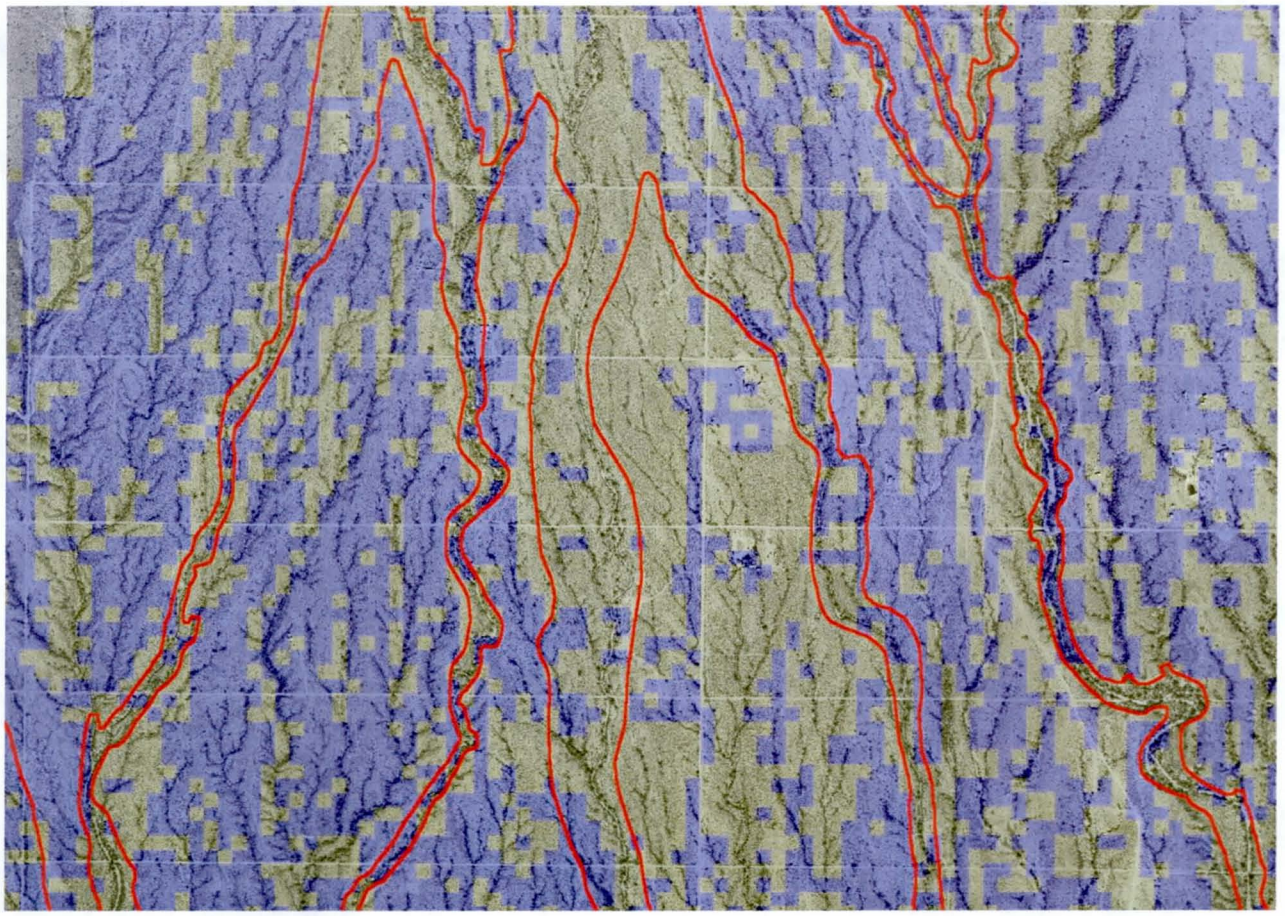

Figure 22

Figure 22 shows a broad area classified as floodprone in the middle third of the figure. The *Approximate FDS* delineated a bifurcating floodplain around a surface with a local tributary drainage network developed on it. This may be an area where the timescales between the 100-year floodplain and the geologic processes used in the expert classifier are highlighted. More well-defined continuous channels in the left and right thirds of the figure appear to be somewhat successfully differentiated by the expert classifier system.

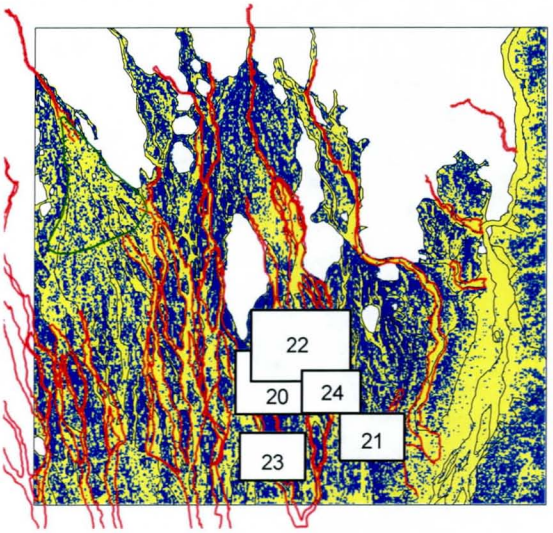

Index Map

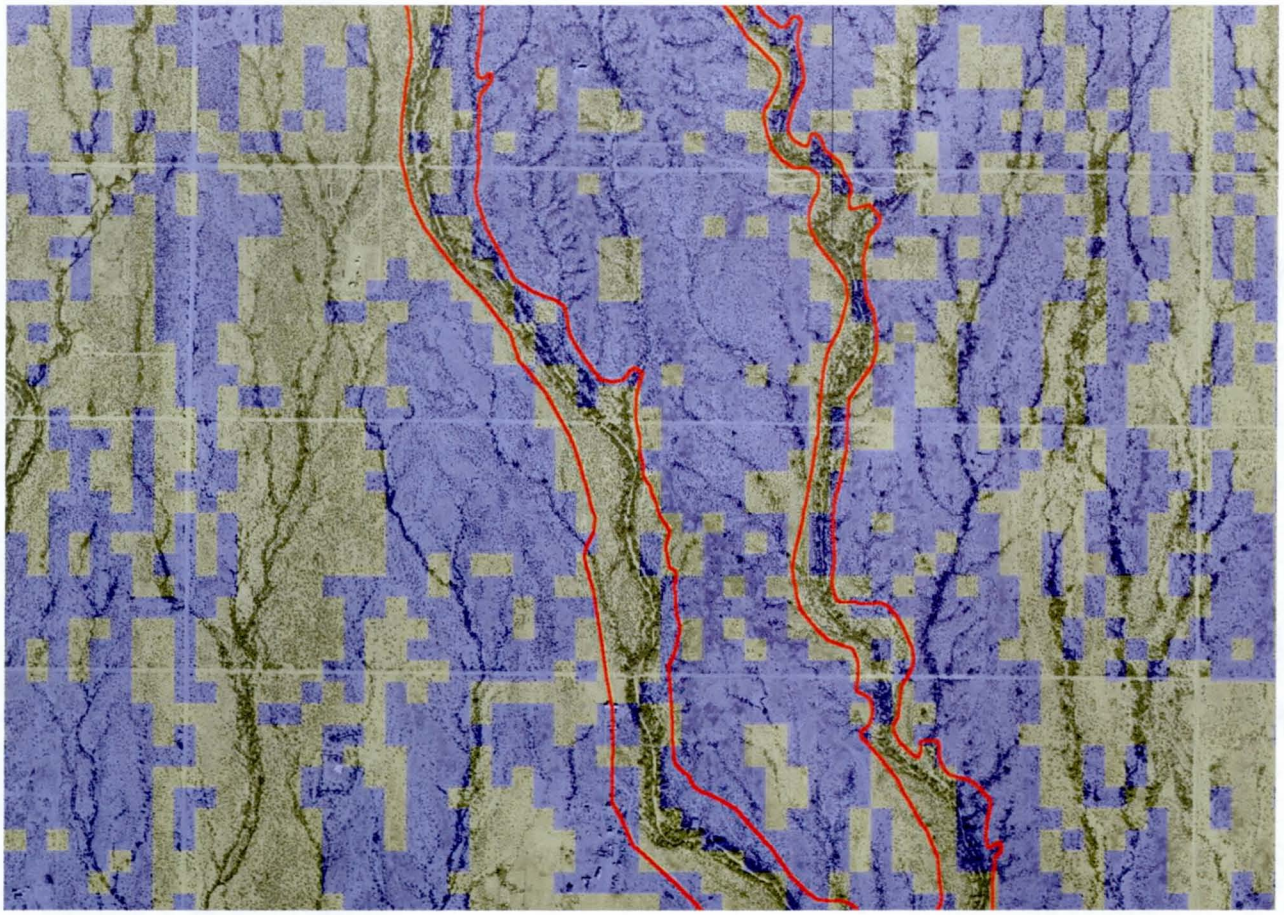

Figure 23

Most of the larger obvious channels seen in Figure 23 were correctly classified by the expert system. Similarly, many of the areas between channels were classified as not flood prone. Not all of the washes were selected for delineation in the *Approximate FDS.*

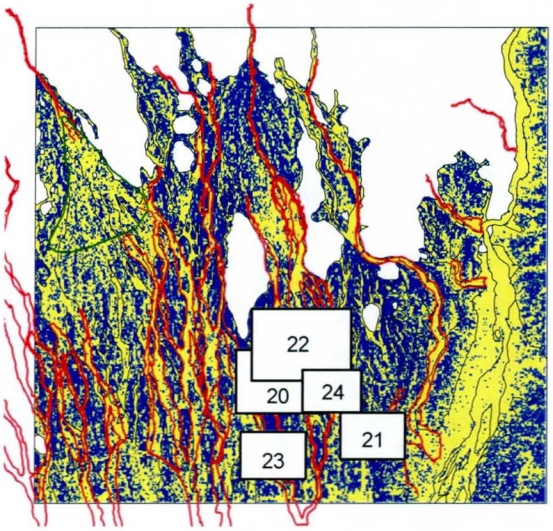

Index Map

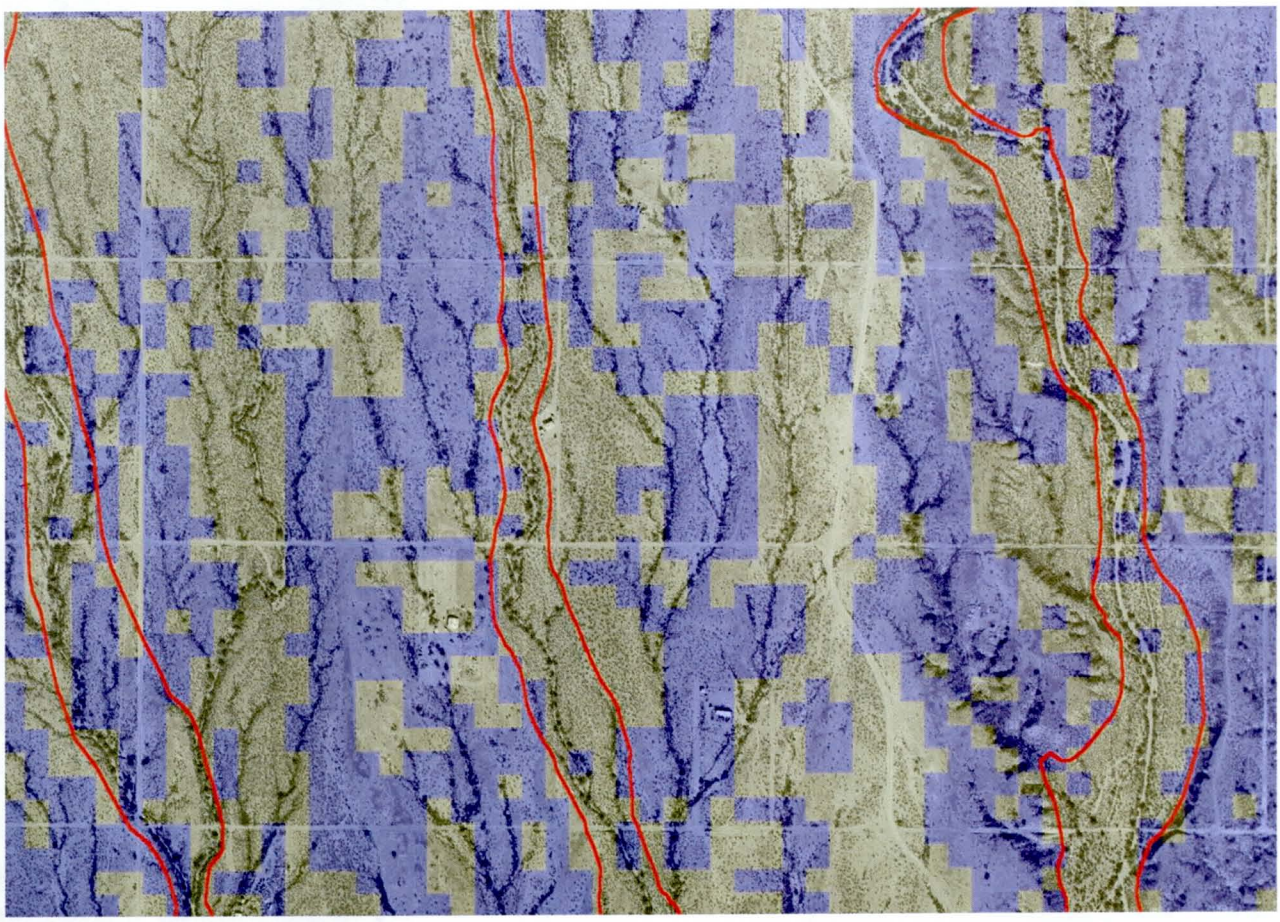

Figure 24

Figure 24 shows generally good agreement between the *Approximate FDS* and the expert system in the areas outlined in red. However, a number of other areas show blue pixels where obvious channels can be seen in the aerial photograph. Some of the yellow areas with visible channels were simply not reaches selected for delineation in the *Approximate FDS*. Finally, the curvy north-south road in the right half of the photo was identified as flood prone. However, it appears to be located along a local ridge top. The bright nature of the bulldozed ground may have "looked" similar to the bright Hassayampa River channel to the expert classifier.

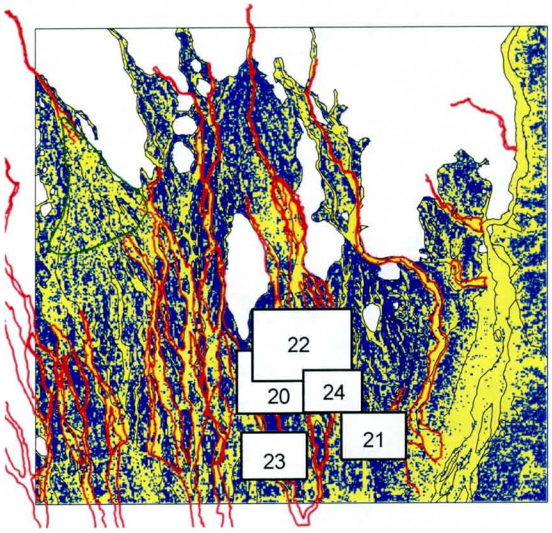

Index Map

These five examples illustrate ways in which the two methods show both similarities and differences in the areas identified as flood prone. Clearly, while there are difficulties applying the remote sensing result to a regulation of flood hazards, it does show the general picture of the location and extent of flood prone areas in the scene.

The area in green in Figure 19 was identified in the Approximate FDS as an area where traditional normal-depth hydraulic approaches are not applicable because it is an alluvial fan. The expert system classifies this area as mostly flood prone with a checkerboard of non-flood prone pixels, accurately reflecting the complex nature of fluvial processes and flood hazards on alluvial fans.

The differences can be explained by the following:

- The horizontal resolution of the digital orthophotos used in the traditional floodplain delineation was 0.3 m (1 foot). Pixels on the Landsat scenes are approximately 30 m (98.4 feet). This difference in horizontal resolution causes spatial discrepancies between the two approaches.
- The 100-year floodplain lines from the *Approximate FDS* were drafted on orthographic 1 foot pixel aerial photographs. The Landsat scenes have approximately 30 m pixels. The accuracy of the registration of the two data sets also causes spatial resolution problems.
- The *Approximate FDS* mapped the one percent chance flood limits. The expert classifier system may be mapping something with a longer time horizon than the one percent chance flood.
- Spectral mixing of of flood prone and non-flood prone characteristics in individual pixels may result in apparent misclassification of any given pixel.
- The ultimate parameterization of the expert classifier system includes judgment of the investigator. The parameters and thresholds selected to differentiate flood prone from non-flood prone areas may result in better or poorer results across the scene.

Level of effort

Estimates for the cost involved in approximate floodplain delineations were approximately $1,800 per mile (based on the 2001 contract) or about 20 hours of labor and expenses per mile. The cost encompasses hydrologic analysis, analysis of the topographic data, simplified hydraulic calculations, floodplain delineation, technical documentation, report production, review by FCDMC and FEMA, coordination, meetings, legal advertising, and other tasks.

The remote sensing procedure, in contrast to the Approximate Zone A delineation methods, requires a significantly smaller amount of time, with a corresponding decrease in the cost. One element of the remote sensing approach that makes unit costs hard to quantify is the spatial coverage. The analysis is for the entire (subsetted) area. That is to say, every 30 m square is evaluated, not just specific reaches of selected watercourses. Using the techniques developed in this study we estimate a similar flood prone / not flood prone image could be developed with about 100 hours of labor for the 72 square mile sub-scene used in this study. About 60-70% of this time would be for the image processing operator and the remainder for the geologist/geomorphologist to assist with field characteristics and surface interpretation. If a polygon geologic map is also desired, an additional 40 hours would be required. The image processing time for the entire 150 km by 150 km Landsat scene would be essentially identical. However, field time and digitizing time, if desired, would require additional effort for the entire scene.

Potential future techniques

The following areas are additional analytical approaches that could be explored in the future to refine the expert classification approach developed in the current study.

Topographic analysis

Incorporation of the available topographic data proved troublesome in this study. Technical solutions to the use of topographic data approached the complexity of traditional floodplain delineation methods. Since the purpose of this project was to demonstrate a more streamlined method of floodplain delineation, the effort to incorporate the topographic data was deemed counterproductive to the goals of the study

Divergence analysis

Band combinations were chosen and used in the mapping based on standard techniques, past experience in similar areas, and specific characteristics of these units. Divergence analysis could quantify which bands are the most useful for these types of regions. Divergence analysis (a type of discriminant analysis) determines which band combination best explains or predicts the geomorphic unit for each pixel.

Deconvolution/target transformation

Due to the large pixel size of Landsat, a pixel spectrum is composed of a mixture of every component on the surface: bedrock, soil type, vegetation, and post-depositional surface changes. This results in regional changes in the spectra of pixels that are mapped as the same geomorphic unit. In other words, two pixels in different regions that exhibit the same post-depositional surface changes, and thus are mapped as the same unit, may have different spectra because the bedrock that also contributes to the spectra is different. Processing techniques exist, namely target transformation and deconvolution, that can "unmix" spectra into its component parts, but these were beyond the scope of this study. They also are more detailed and time intensive, which does not support the goal of this project, namely the ability to process this data quickly to produce geomorphic maps efficiently.

Summary and conclusions

Multi-spectral remote sensing datasets provide additional information beyond aerial photographs to differentiate geomorphic surfaces and flood prone areas. This study has yielded the following results:

1. Differences in pixel spectra do represent differences in ground characteristics.
2. These differences are clearly identified in multiple band combinations.
3. The use of multiple band combinations can provide an efficient way to identify different geomorphic units and delineate boundaries between them.
4. An expert classification system can be developed to discriminate between flood prone and non-flood prone areas.
5. The spatial resolution of Landsat data is inadequate for the purposes of floodplain management at the individual lot level of detail.
6. The expert classification scheme developed in this study could be applied to other areas in Maricopa County as a relatively time and cost efficient method of broadly defining flood prone areas.
7. The utility of the remote sensing approach outlined in this study is limited for floodplain managers.

8. Used in conjunction with other traditional geologic and engineering approaches, remote sensing can provide helpful information to identification of flood hazards on arid and semi-arid piedmonts in central Arizona. In particular, significant flow corridors may be able to be identified. Also, alluvial fan areas where the *Piedmont Flood Hazard Assessment Manual* is applicable may also be able to be identified.

References

Birkeland, Peter W.,1984, *Soils and geomorphology*, Oxford University Press, New York.

Blair, T.C. and McPherson, J.G., 1994, Alluvial Fan Processes and Forms, *in* Geomorphology of Desert Environments, edited by A.D. Abrahams and A.J. Parsons, Chapman Hall.

Bull, William B.,1991, *Geomorphic responses to climatic change*, Oxford University Press, New York.

Cooke R.U. and Warren A., 1973, *Geomorphology in Deserts*, University of California Press, Los Angeles.

Dempsey, K.A., 1988, Geologic map of Quaternary and upper Tertiary alluvium in the Phoenix North 30' x 60' quadrangle, Arizona, (revised August 1990).

Dixon, J.C., 1994, Aridic Soils, Patterned ground, and desert pavements, *in Geomorphology of desert environments*, (eds. A.D. Abrahams and A.J. Parsons), Chapman & Hall, London.

Dorn, R.I., 1991, Rock Varnish, *American Scientist*, 7, 542-553.

Elachi C., 1987, *Introduction to the physics and techniques of remote sensing.* Wiley, New York.

Farr, T.G. and Chadwick, O.A., 1996, Geomorphic processes and remote sensing signatures of alluvial fans in the Kun Lun Mountains, China, *Journal of Geophysical Research*, v. 101, no. E10, 23091-23100.

Field, J.J. and Pearthree P.A., 1997, Geomorphic flood-hazard assessment of alluvial fans and piedmonts, Journal of Geoscience Education, 45, 27-37.

Franklin, J, Duncan, J, and Turner, D.L., 1996, Reflectance of Vegetation and Soil in Chihuahuan Desert Plant Communities from Ground Radiometery using SPOT Wavebands, *Remote Sensing of the Environment*, 46, 291-304.

Gillespie, A.R., Kahle A.B., and Palluconi, F.D., 1984, Mapping alluvial fans in Death Valley, California, using multichannel thermal infrared images, *Geophysical Research Letters*, vol. 11, no. 11, 1153-1156.

Gillespie, A.R., 1992, Spectral mixture analysis of multispectral thermal infrared images, *Remote Sensing of the Environment*, 42, 137-145.

Gober, P and E. K. Burns, in press, The size and shape of Phoenix's urban fringe. *Journal of Planning Education and Research.*

Gober, P. E., E. K. Burns, K. Knowles-Yanez and J. James, 2000, Rural-to-urban land conversion in metropolitan Phoenix, in *Arizona Policy Choices*, edited by: J. S. Hall, N. J. Cayer, and N. Welch.40-45. Morrison Institute for Public Policy, Arizona State University, Tempe, AZ.

Hunt, G.R., 1980, Electromagnetic radiation: the communication link in remote sensing, *in Remote Sensing in Geology* (eds.. B.S. Siegal and A.R. Gillespie), pp 5-45, J. Wiley & Sons, New York.

J.E. Fuller/ Hydrology & Geomorphology, Inc., in-progress, Approximate Floodplain Delineation Study for Watershed OO, under preparation for the Flood Control District of Maricopa County, FCD 200C019.

Jensen, John R., 1996, Thematic Information Extraction: Image Classification, *in Introductory Digital Image Processing: A Remote Sensing Alternative*, Prentice Hall.

McAuliffe, J.R., 1994, Landscape Evolution, soil formation , and ecological patterns and processes in Sonoran desert bajadas, *Ecological Monographs*, 64(2),111-148.

McFadden L.D., Ritter J.B. and Wells, S.G., 1989, Use of multiparameter relative-age methods for age estimation and correlation of alluvial fan surfaces on a desert piedmont, eastern Mojave Desert, California, *Quaternary Research,* 32, 276-290.

McFadden, L.D., Wells, S.G. and Jercinovich, M.J., 1997, Influences of eolian and pedogenic processes on the origin and evolution of desert pavements, *Geology*, 15, 504-508.

National Research Council (NRC), 1996, *Alluvial Fan Flooding*, National Academy Press, Washington D.C..

Ramsey, M.S., 1996, Quantitative Analysis of Geological Surfaces: a deconvolution algorithm for mid-infrared remote sensing data, 276 pp. Ph.D. dissertation, Arizona state University, Tempe.

Robinson, S.E. and Arrowsmith, J R., in press, Using Remote Sensing Analysis to Map the Western White Tank Mountains, AZGS Open File Report.

Sabins, F.F, 1997, *Remote Sensing: Principles and Interpretation*, W.H. Freeman and Company, New York.

Appendix 1: Choosing and ordering data

Choosing a data set depends on the spatial and spectral requirements of the project goals. Remote sensing data can be grouped into three spectral classes—multi-spectral, hyper-spectral and radar—and is either acquired from an airborne or satellite platform. Multi-spectral data has on average 5-9 spectral bands, while hyper-spectral data has upwards of 150 spectral bands. Hyper-spectral data has the advantage of producing detailed spectra that approximate laboratory spectra allowing for more precise identification of surface materials. However, currently there is no satellite platform acquiring hyper-spectral data, so the spatial coverage is spotty and repeat coverage of an area is rare. Hyper-spectral data, due to its increased number of bands, is more cumbersome to work with than multi-spectral data. Radar data is acquired through an active sensor system, as opposed to the passive system of Landsat, and is typically the most expensive type of data. Radar data requires some processing to extract quantitative characteristics, but many of the remote sensing modules have radar modules to aid in this processing.

Most remote sensing data can be found on the EDC data web site (http://edcdaac.usgs.gov/main.html). This site is available to be searched as a guest. The search engine screen allows for latitude/longitude searches and specifying the sensor and data-processing level desired. Radar data can be searched for through the SPOT corporation of EURIMAGE> The actual satellite web pages (ERS< JRS< RADARSAT) do not sell their own data.

The following is a list of characteristics of various spectral data sources to help with data selection:

Landsat
1. Easy to obtain
2. Long term temporal coverage
3. Covers every place on the earth every 16 days
4. 6 bands in the visible and near infrared
5. 1 band in the thermal
6. 1 panchromatic band
7. Most commonly used remote sensing data

ASTER
1. Spotty spatial coverage currently, will have global map in 5 years
2. No blue band
3. Two bands in the visible
4. 6 bands in the SWIR
5. 6 bands in the thermal
6. Must get level 1b data, level 1a is too raw to make it worth using except to make pretty pictures

Radar
1. Active sensor vs. passive
2. Expensive
3. Best is SIR-C if available because it has multiple bands and multiple polarizations
4. Most common RADASAT and ERS each just C band with one polarization

AVIRIS

1. Hyperspectral data
2. 244 bands in the VIS and SWIR
3. Airborne sensor so variable spatial and temporal coverage

Appendix 2: Data ordered for this project (FCD2000C013, Task 9)

Landsat ETM+ Scene 1—data taken from header file

1. Scene Specific Information
   - Date: November 11, 1999
   - L71037037_03719991111
   - Path: 37, Row: 37
   - Sun elevation angle 36.1
   - UTM projection
   - Ellipsoid WGS84
   - Datum WGS 84
   - USGS Map Zone: 12
2. Visible, Near Infrared (HRF) data type/size
   - Rows: 7241
   - Columns: 8241
   - Bands: 6
   - Unsigned 8-bit data
3. Thermal (HTM) Data type/size
   - Rows: 3621
   - Columns: 4121
   - Bands: 2
   - Unsigned 8-bit data
4. Panchromatic (HPN) data type/size
   - Rows: 14481
   - Columns: 16481
   - Bands: 1
   - Unsigned 8-bit data

Scene 1 Geographic Information

	Latitude	Longitude	UTM Easting (X)	UTM Northing (Y)
Upper Left	1135303.9996W	340756.7941 N	234000.00	3780600.00
Upper Right	1111214.3137W	340958.2243N	481200.000	3780600.00
Lower Right	1111158.1467W	321225.2682N	481200.00	3563400.00
Lower Left	1134915.7520W	321032.5239N	234000.000	3563400.00

Landsat ETM+ Scene 2—data taken from header file

- Scene Specific Info
- Date: March 2, 2000
- Order Number: L71037037_03720000302
- Path: 37, Row: 37
- Sun elevation angle: 42.7
- Projection Information
- UTM projection
- Ellipsoid WGS84
- Datum WGS 84
- USGS Map Zone: 12
- Visible, Near Infrared (HRF) Data type/size
- Rows: 7241
- Columns: 8241
- Bands: 6
- Unsigned 8-bit data
- Thermal (HTM) Data type/size
- Rows: 3621
- Columns: 4121
- Bands: 2
- Unsigned 8-bit data
- Panchromatic (HPN) data type/size
- Rows: 14481
- Columns: 16481
- Bands: 1
- Unsigned 8-bit data

Scene 2 Geographic Information

	Latitude	Longitude	UTM Easting (X)	UTM Northing (Y)
Upper Left	340738.9827N	1135153.1524W	235800.000	3780000.000
Upper Right	340938.8553N	1111103.9650W	483000.000	3780000.000
Lower Right	321205.8851N	1111049.3498W	483000.000	3562800.000
Lower Left	321014.5877N	1134806.5033W	235800.000	3562800.000

Radar Data

- Scene Specific Info
- Date: May 27, 2000
- Order Number : 4933001
- Orbit 26677, Frame: 2925
- UTM projection
- Ellipsoid WGS84
- Datum WGS 84
- USGS Map Zone: 12
- Visible, Near Infrared (HRF) Data type/size
- Rows: 10100
- Columns: 9800
- Bands: 1
- Unsigned 16-bit data

Radar Data Geographic Information

	Latitude	Longitude	UTM Easting (X)	UTM Northing (Y)
Upper Left	34.4281287	-113.516219	268750	3812500.00
Upper Right	34.4483002	-112.1838377	391250	3812500
Lower Right	33.3098798	-112.1682181	391250	3686250
Lower Left	33.2905511	-113.4833514	268750	3686250

All of these files are provided on CD-ROM supplied to the FCDMC along with this report.

Appendix 3. Preprocessing Steps in ERDAS Imagine

This project used ERDAS Imagine 8.4 with the Atcor2 module on a Unix Platform. The main

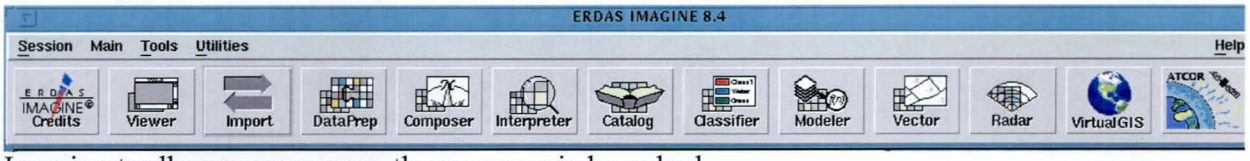

Imagine toolbar appears once the program is launched.

Importing Landsat Data

1. Copy all the files from the EROS data center CD to the platform with Imagine
2. Select the Import Button from the Main Imagine Toolbar and set the follwing in the Import/Export window that pops up.

- Set Type to Landsat-7 fast-L7A EROS
- Set Media to File
- Use the directory buttons to select the correct header file. Note that the import functions operates off the header files, not the individual band files. Choose a filename ending in one of the following:
- _HPN.FST File for the panchromatic band (#8)
- _HRF.FST file for the Visible and Near Infrared (#1-5,7) bands
- _HTM.FST file for the thermal bands (#6.1,6.2)
- Enter an output file name
- Check to make sure all the information displayed in the next window is correct such as the geographic projection, number of bands, etc. This information is read from the header file.
- When importing from the HRF header there should be 6 bands, pixel size = 30
- When importing from the HPN header there should be 1 band, pixel size = 15
- When importing from the HTM header there should be 2 bands, pixel size = 60
- Hit Okay

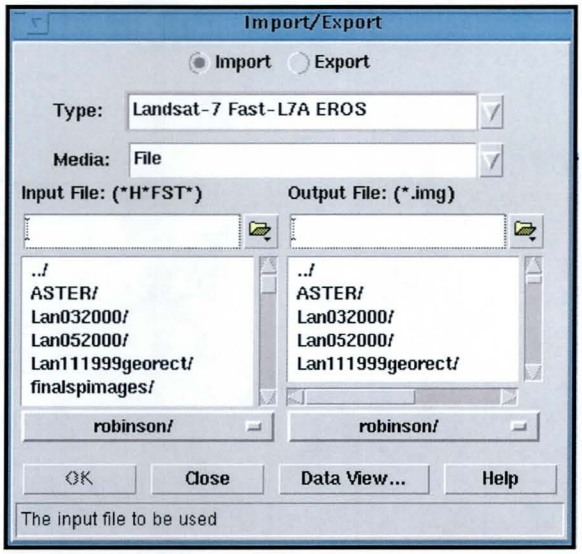

Radar Importing Processing Steps

1. Copy all the files from the EROS data center CD to the platform with Imagine
2. Select the Import Button from the Main Imagine Toolbar and set the following in the Import/Export window that pops up.

- Set Type to ERS(I-PAF CEOS)
- Set Media to File
- Use the directory buttons to select the correct header file. Note that the import function operates off the header file, not the data files. Choose the file that has the suffix .DAT
- Enter an output file name
- Hit Okay

Subseting image

To make future processing steps faster, subsets should be made of each of the images of the region of interest. The original Landsat scene covered the entire metropolitan Phoenix area and surrounding regions. For this project we subset a smaller region from the larger image that was only ~14 by 14 kilometers.

Subseting an Image Processing Steps

1. Select the data preparation button from the main Imagine toolbar.
2. Select the subset image option.
3. Select your original full dataset as your input file.
4. Select an output file name.
5. Type in the coordinates directly into the boxes or choose select from the inquire box.
   - You will be directed to click in the window of the image you want to subset.
   - Drag and enlarge the box until it encompasses the area you want by grabbing the corners and sides.
6. Transfer the corresponding coordinates that appear in the inquire window to the Subset window.
7. Make sure you check that both the inquire box and the subset box are set to either map or file.
8. Choose the output type (this should be set automatically to the original file type).

- For Landsat the data is unsigned 8-bit and the output continuous.
- For ERS radar the data is unsigned 16-bit and the output continuous.

9. Choose the number of layers you want to include in the subset
10. Select Okay

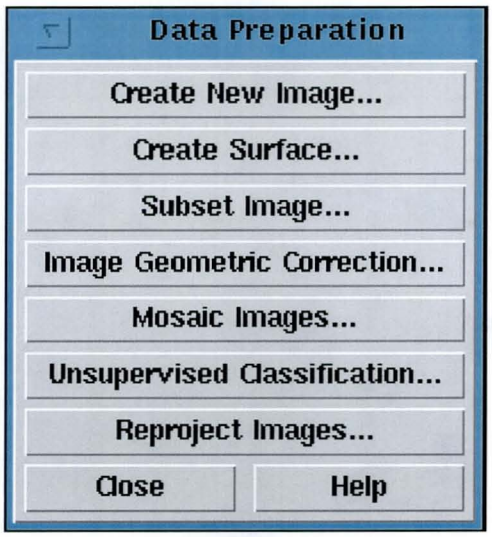

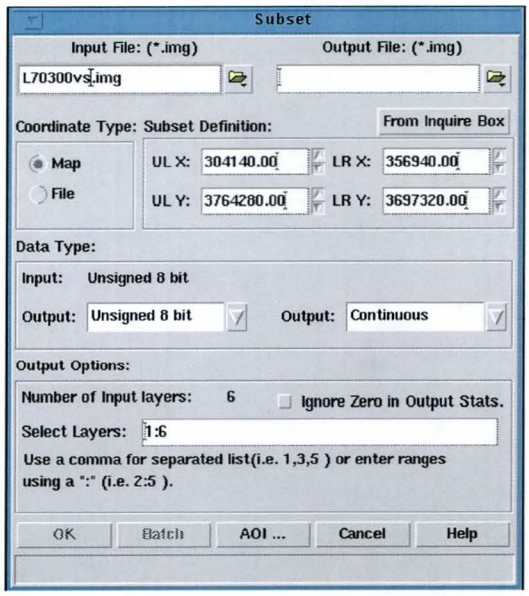

Atmospheric Correction and conversion to reflectance values

The DN values of a Landsat pixel represent not only the amount of radiation reflecting off the surface material, but also the interaction of that radiation with the atmosphere, and a scaling conversion by the satellite. The Landsat satellite is actually measuring the number of photons in a given wavelength region. The number of photons received is a combination of not only the radiation reflecting off the surface controlled by the material properties (the parameter we are interested in) but also photons that are derived from the radiation passing through the atmosphere. This atmospheric component is removed so that image pixel spectra can be compared with lab spectra (which do not have an atmospheric component) and so that image pixels can be compared between scenes taken on different days with different atmospheric characteristics.

The number of photons recorded by the satellite for a given wavelength is scaled to a number between 0 and 255 so that the information can be transferred as 8-bit data. By using characteristics of the satellite, we can convert this scaled DN value, which has no real-world units, to percent reflectance, which represents a material property of the surface.

The Imagine ATCOR module was used to remove the atmospheric component and convert the DN values to percent reflectance values. You want to run ATCOR on any visible or near infrared imagery.

Atmospheric Correction Processing Steps

1. Before running ATCOR you must have statistics for the image with a skip factor of one
   - Typically to save processing time, Imagine calculates statistics with a skip factor
   - To recalculate statistics open up the input image in a viewer
   - Select the *i* icon in the viewer toolbar
   - Select the Greek Sum Sign in the Information toolbar
   - Change the skip factor in the recalculate statistics window to 1
   - Hit Okay

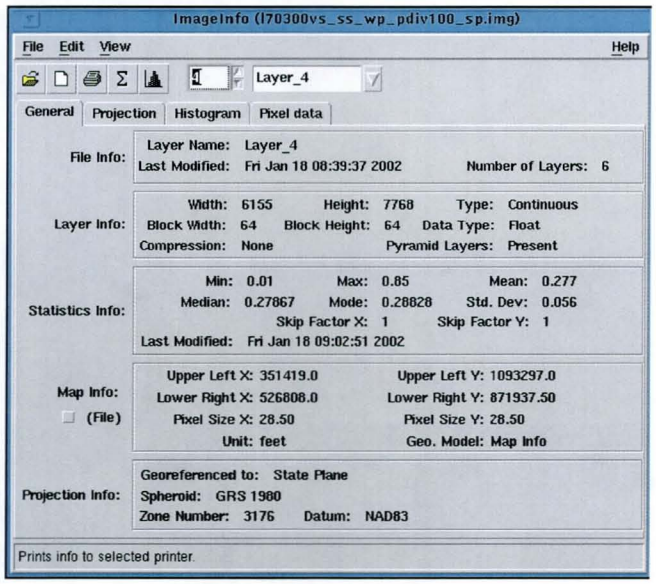

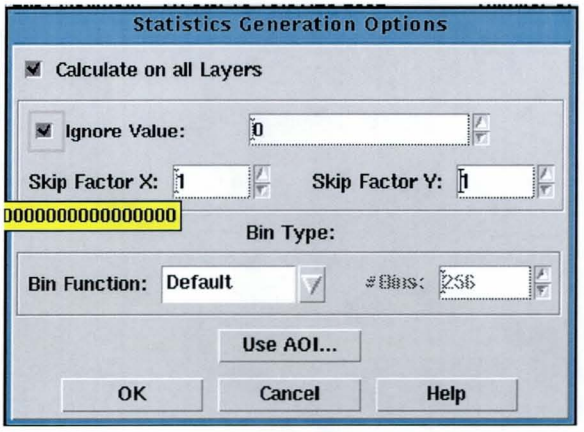

2. Select the ATCOR icon from the main imagine toolbar or select it under the Main file menu.
3. Select the Start ATCOR2 button.

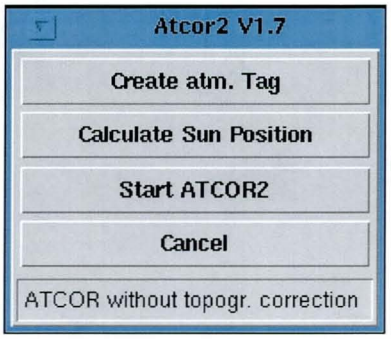

4. Enter your input dataset (this is the original or spatially subsetted Landsat file with pixel values in DN's).
5. If you have separated out the thermal band from the Visible and SWIR (i.e. your input dataset is only 6 bands) change the band 6 window to band 7 [you are skipping band number 6 in the dataset because that is the thermal band].
6. A gains settings window will open. These gains do not refer to the gains and biases in the Landsat header, they refer to the High/Low gain setting of the instrument in each band. Refer to the Landsat User's web page (http://landsat7.usgs.gov) to determine the setting for each

band for a given scene. Once these gains have been set, Hit okay and you will return to the main Atcor2 page.

- High gain bands set to 1.5
- Low gain bands set to 1
- High gain thermal bands are set to 2 NOT 1.5

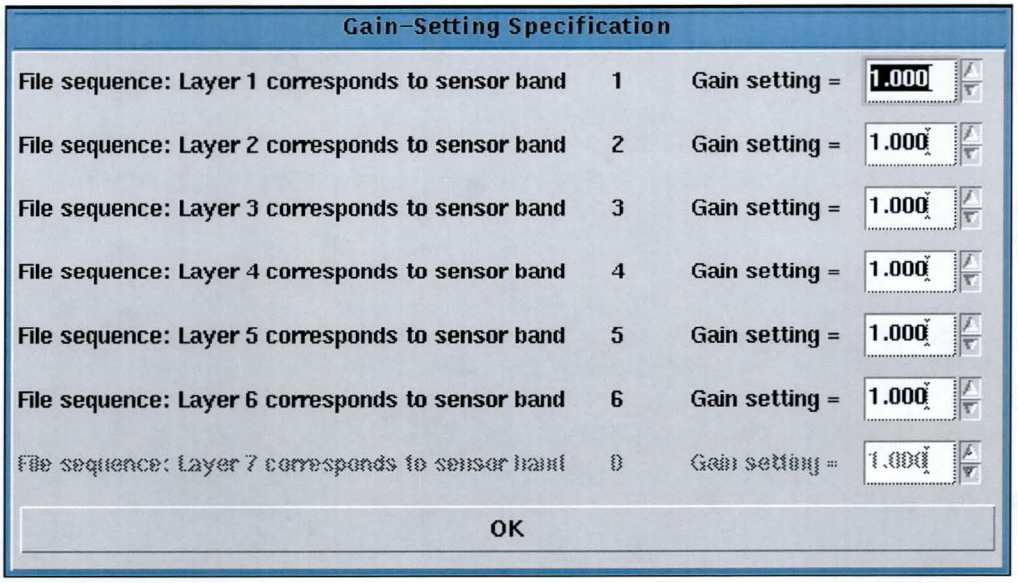

7. Select the etm.cal calibration file. Imagine should go to the right folder automatically, but if not this file is in /opt/imagine/840/etc/atcor/cal/tm7/etm.cal
8. Select and atmosphere appropriate to your scene. For this project I selected the "arid atmosphere, desert aerosol" model for the atmospheric model
9. Set the visibility, ground elevation, and solar zenith angle for the scene.
   - A visibility of 25 km was used for this project as this is the visibility at Sky Harbor Airport on a clear day (Will Stefanov, personal communication).
   - A ground elevation of 0.45 km (~1800 ft) was used.
   - The solar zenith angle is the same as the solar elevation angle and can be found in the Landsat header files for each scene.
10. Set the reflectance factor
    - The default is 4 but that means a maximum of 63% (255/4) reflectance. In arid and urban scene reflectance can be higher so I set the reflectance factor to 3 to give a max possible reflectance of 85% (255/3). This decision was made because with a reflection factor of 4 the histograms for bands 5 and 6 were cut off at the 255 mark with a spike in the number of values at 255.
11. Select the ATCOR module you wish to use
    - I selected constant atmosphere because it is the simplest
    - I then used the no haze module in the window that appears
12. Select Run model

13. The result should be an image with values still between 0 and 255. Divide the values in your image by the reflectance factor and you will have % reflectance (ex) reflectance factor=3, DN value =255, resulting value = 85 e.g. 85 % reflectance.

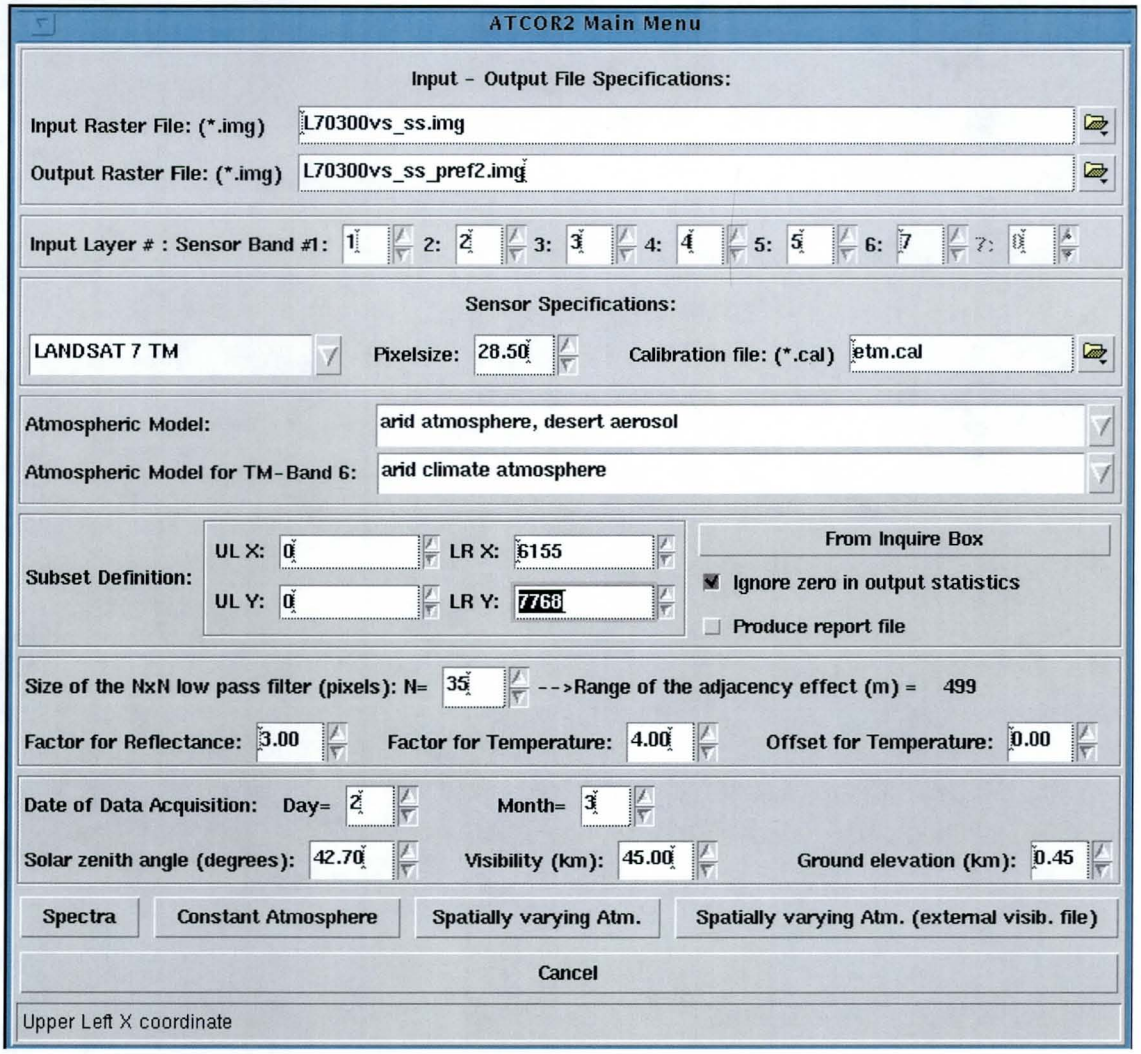

14. A Reflectance factor of 3 was used instead of the standard 4. Reflectance factors are used so that the data can be displayed as 8bit data as integers from 0 to 255. With a reflectance factor of 4, the highest percent reflectance allowable is 63.75% (255/4). If a scene has higher reflectances the reflectance factor must be reduced. In this scene the Hassayampa River had very high reflectances, so the reflectance factor was changed to 3 allowing for a maximum reflectance of 85% (any reflectances between 85 and 100 would be displayed as 85).
15. In examining the resulting histograms, only in band 5 were many values hit the 85% maximum boundary.
16. The resulting values are then divided by 100 to convert to percentages so they can be compared to other spectra from both lab and imagery. Percent reflectance is the standard unit for these data.

Registration

The original data ordered for this project was georeferenced by the EROS data center, Level 1G. However, on comparison to other georeferenced data, the Landsat data was "off" by up to 1/2 kilometer. The March 2, 2000 scene was georeferenced by image to image registration using the November 1999 images ordered by the AZGS that were a higher level product with georeferencing of greater accuracy. The AZGS data are also included in the CD-ROM disks provided with this report.

Appendix 4. Image Processing

Band Algebra

The ModelMaker Module can be used in imagine to calculate indices such as NDVI and perform any necessary band algebra. Model maker can be selected from the main imagine toolbar. Select Model Maker from the window that pops up. The following models were created for this project:

1. Atcortopref.gmd
   - This model divided the resulting DN's from the Atcor2 module by 100 to convert the pixel values to percent reflectance
2. Ratiostd.gmd
   - This model calculated all of the standard indices-NDVI, SAVI, clay, iron, and opaques
3. Ratioss.gmd
   - This model calculated all of the scene specific indices
4. Merfefinalus.gmd
   - This model merged the outputs of Ratiostd, ratioss, atcortopref and prinicipal component analysis into one image consisting of 23 bands. By combining all the bands into one image, band combinations could be made using any of the ratio, TM reflectance bands, or principal components

Converting Atcor DN values to percent Reflectance

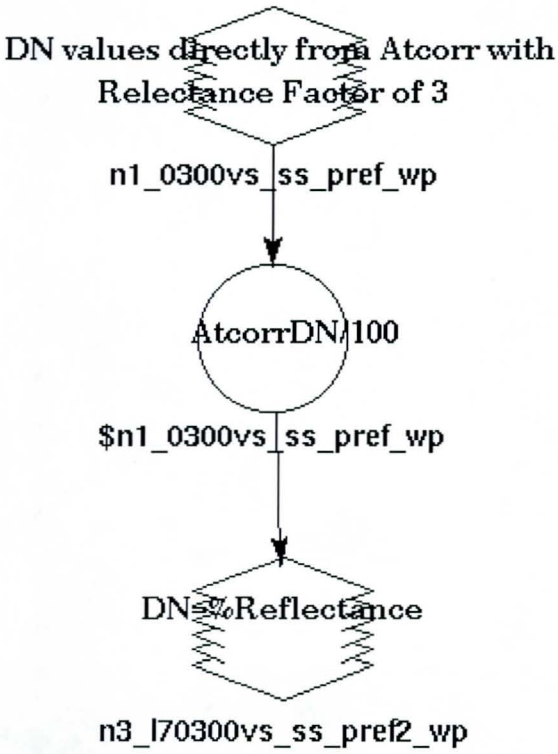

MergeFinalus

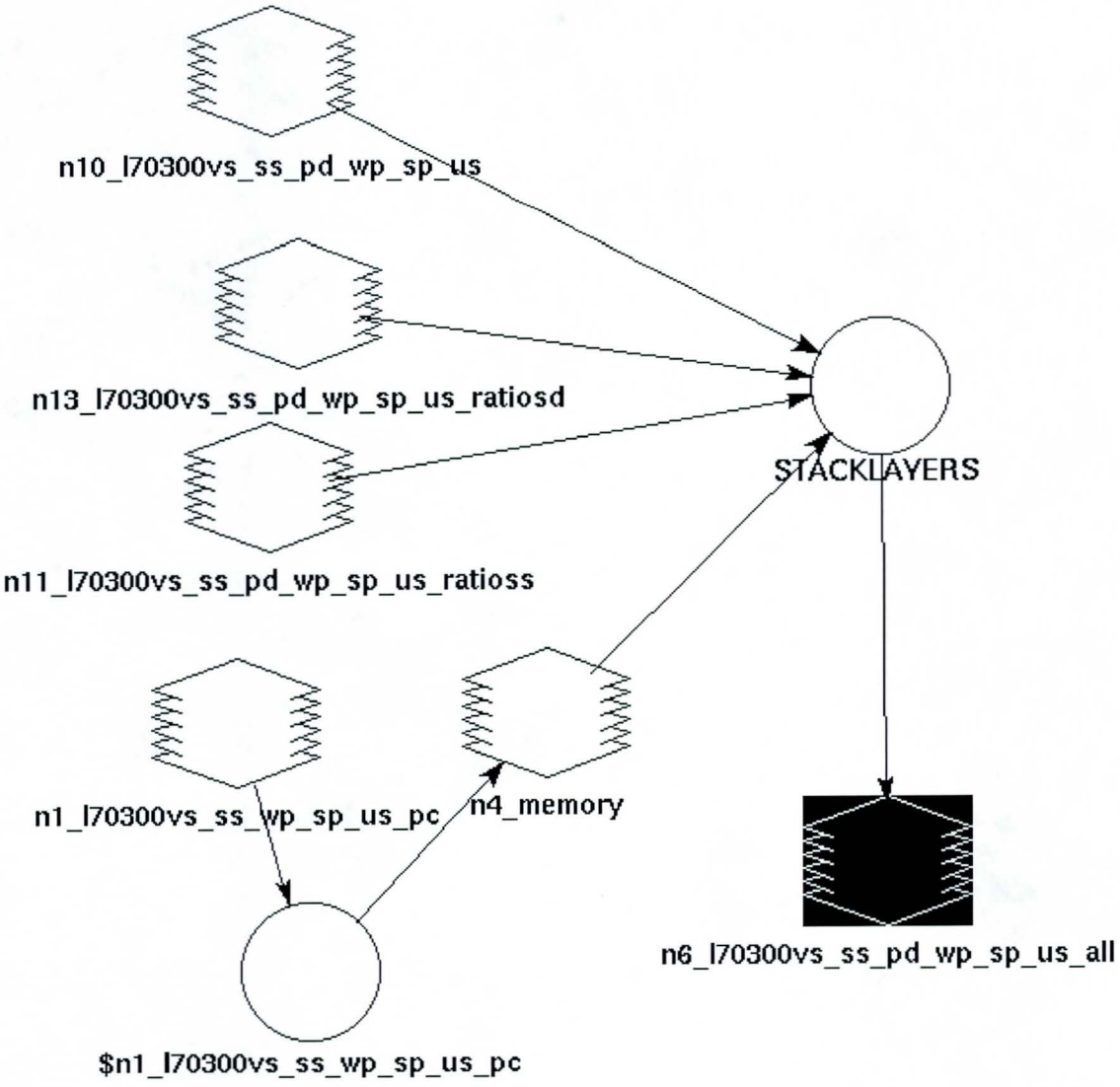

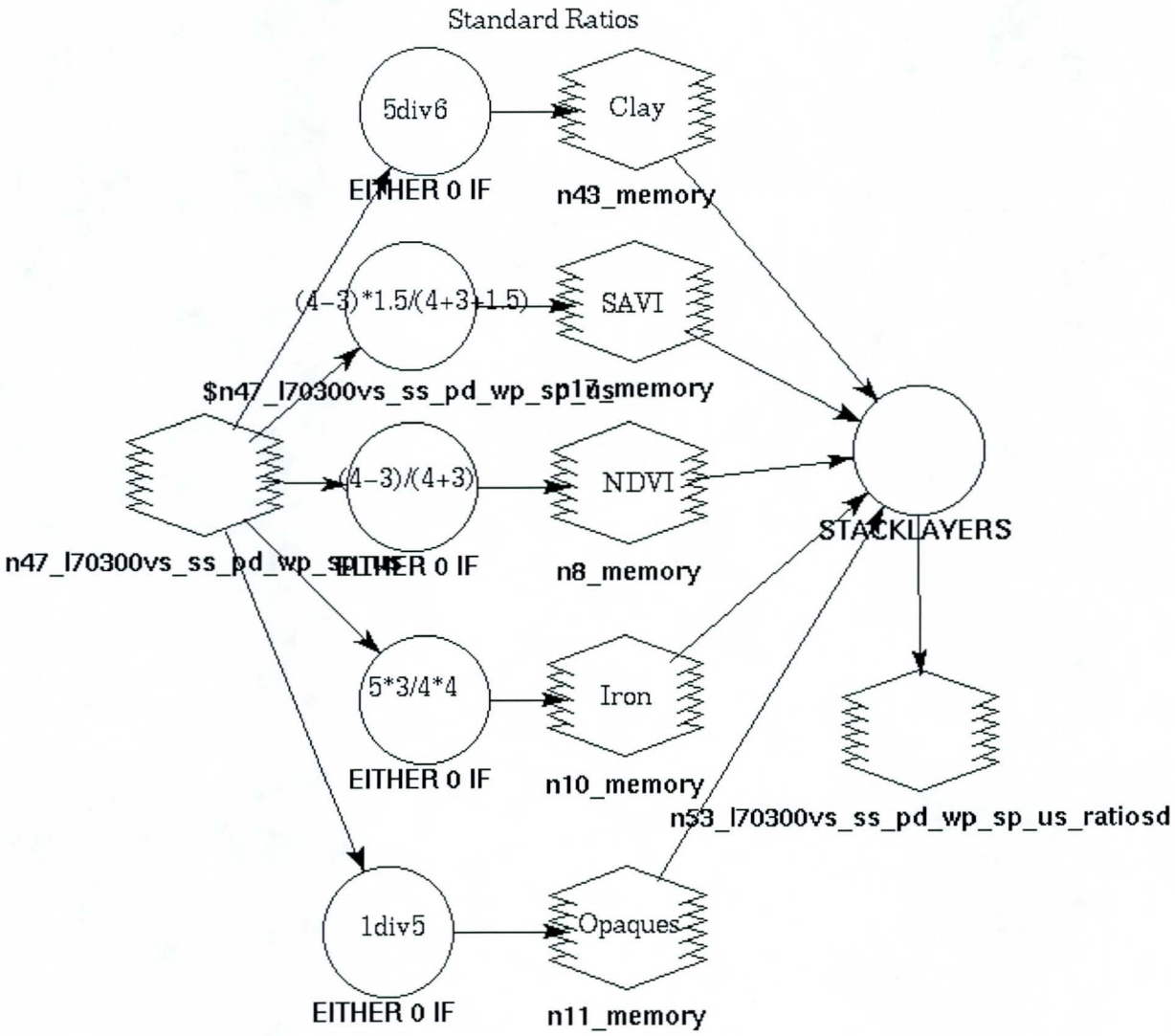
Standard Ratios
5div6
Clay
EITHER 0 IF
n43_memory
(4-3)*1.5/(4+3+1.5)
SAVI
$n47_l70300vs_ss_pd_wp_sp1us
memory
(4-3)/(4+3)
NDVI
n47_l70300vs_ss_pd_wp_sp
EITHER 0 IF
n8_memory
STACKLAYERS
5*3/4*4
Iron
EITHER 0 IF
n10_memory
n53_l70300vs_ss_pd_wp_sp_us_ratiosd
1div5
Opaques
EITHER 0 IF
n11_memory

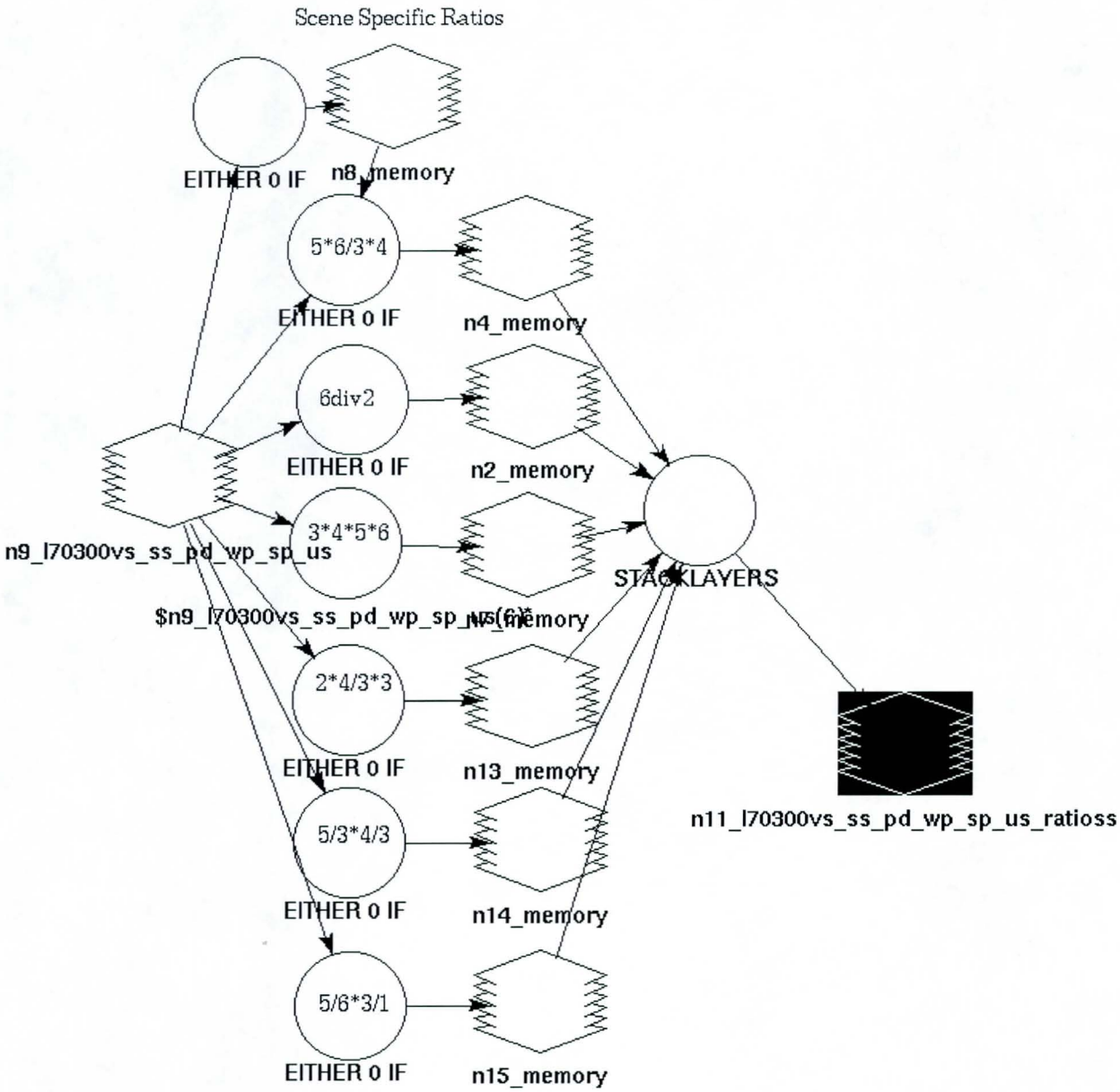
Scene Specific Ratios
EITHER 0 IF
n8_memory
5*6/3*4
EITHER 0 IF
n4_memory
6div2
EITHER 0 IF
n2_memory
3*4*5*6
n9_l70300vs_ss_pd_wp_sp_us
STACKLAYERS
$n9_l70300vs_ss_pd_wp_sp_us(6)
n5_memory
2*4/3*3
EITHER 0 IF
n13_memory
n11_l70300vs_ss_pd_wp_sp_us_ratioss
5/3*4/3
EITHER 0 IF
n14_memory
5/6*3/1
EITHER 0 IF
n15_memory

Appendix 5. Generating Geologic Map

Creating Vector Map

1. Imagine has a vector module that can be used to draw vector creating a polygon based map through on-screen digitization.
2. Open a viewer and display a raster image that is to be used as the back drop for drawing the map. You can have multiple viewers open with different band combinations and display the vector layer on top of each of them. As you make changes to the vector layer in one window those changes will also be displayed in the other viewers.
3. Open a new vector layer by choosing "New" under the file menu and selecting Vector. Input the new vector layer name.
4. Select "enable editing" under the vector menu. This allows changes to be made to the vector layer.
5. Select "tools" under the vector menu to display the vector tools.
6. Select "options" under the vector menu to set your tolerances for Nodesnap, Arc snap and weed.
7. Once set use the line and polygon tools to begin tracing unit boundaries on the screen.
8. After you have digitized a few polygons/arc, save your work by selecting save under the file menu.
9. Select the vector module from the main imagine toolbar.
10. Select "build" vector layer topology or "clean" to update topology.
11. Reopen vector layer in window.
12. Select "viewing" properties from the vector menu in the viewer.
13. Here you can determine which attributes you are displaying, including node errors that alert you to unclosed polygons.
14. Select "attributes" under the vector menu. This menu allows you to change the attribute file of the layer including adding a column to assign geologic unit labels. It also allows you to select all polygons with given attributes to check that you have assigned the correct attributes to the correct polygon.
    - To add a column, select "column attributes" under the edit menu. Select new column and define its characteristics. Once you hit okay, the new column should appear the in the attribute spreadsheet. To change the value in a cell, click on it and enter the value and hit return. Unless you hit return the value will not be entered.
    - To select and display those polygons with a given attribute, select "select rows by criteria" under the edit menu. Use this to select rows by a given attribute value. For example unit==2, will select and display all polygons with a value of 2 in the units column.
15. Remember to build or clean your coverage after you save it and before exporting.

Exporting coverage to .e00 or shape file

To export a coverage to be read by ArcINFO or ArcView:

1. Select the Import Button from the main Imagine toolbar.
2. Click the export button.
3. Select either "coverage to arc-interchange file" to produce a .e00 file or "shape file" from the file type menu.
4. Select the coverage to export in the left window and the export name in the right.
5. Click okay.

Displaying pixel spectra

To display pixel spectra:

1. Open a viewer and display a multi-band image.
2. Select "profile tools" from raster menu.
3. Select "spectral" in the pop up window and hit okay.
4. Use the cross hair icon in the top of the spectral profile viewer menu. This turns the cursor into a cross hair when in the viewer window.
5. Click on the pixel of interest.
6. A spectra will appear in the spectral profile viewer.
7. You can change the coordinates that appear in the upper right portion of the window from file to map if you want to know the geographic location of each point. As yet I have not found how to save this geographic information with the spectra, so if you want to reoccupy this specific site, write down the geographic info.
8. For some reason imagine displays the first spectra in red and all following in shades of green which makes it hard to differentiate them. To assign specific names and colors to pixels:
   - Select "chart legend" from the edit menu in the spectral profile viewer window.
   - Right click on the color boxes to change the color.
   - Select the cell under Name and type in new name. Remember to hit return or the change will not be accepted.
9. To change the display of the profile window:
   - Select "chart options" from the edit menu in the spectral profile viewer window.
   - Here you can change the range of bands displayed under x axis options, the y axis range, and the decimal places of the axis labels in the "format" cell under x and y axes options.
10. You can display the numeric information about the spectra by selecting "tabular data" under the View menu.
11. This tabular data can be exported to a text file that can be read by Microsoft Excel.
    - Select "export data" under the file menu in the spectral profile viewer window.

Calculating polygon statistics

To determine the unit signature, as compared to an individual pixel signature described above:

1. Select the vector module from the Main imagine toolbar.
2. Select Zonal attributes from the vector Utilities menu.
3. Enter the Polygon coverage name in the upper left window and the raster image name in the upper right that the spectral information is to be taken from.
4. Select the layer to calculate the statistics from.
   - Unfortunately Imagine does not calculate the statistics for each layer in an image automatically, you must run the zonal attributes for each layer individually.
5. Select the zonal functions of interest (max, min, mean, etc.).
6. Type in a name for each function that will be the column name in the attribute file of the coverage. Indicate in the name which image layer the statistics are for ie MaxTM1.
7. Hit okay
8. Open the vector layer in a viewer, select "vector attributes" from the vector menu in the viewer.
   - You should see new columns with the names entered in the zonal attributes window. Sometimes this takes a little time to update (~1 minute) so if the columns are not there immediately, open the attributes again in about a minute.

Subsetting an Image from an AOI.

In this project we wanted to remove the bedrock from the image for the Expert classification system which was focused on the Quaternary units. Once we had created the geologic vector map and assigned unit designation to each polygon, we could select all those polygons that are not bedrock and create a new image with no bedrock

1. Open geologic map in viewer.
2. Select "attributes" under vector menu in the viewer.
3. Select "select rows by criteria" under the edit menu in the attribute window.
4. Use the "=!" to select all units that are not bedrock.
   - For example, if the bedrock unit designation was 2, entering unit=!2 would select all polygons that are not designated bedrock.
5. Under the AOI menu in the viewer select "copy selection to AOI."
   - Make sure that the selected polygons are highlighted when you do this, if they are not it might be because you have not selected to display the polygons under the viewing attributes menu. You must also "enable editing" under the vector menu to select rows.
6. Once the selection has been copied to the AOI, select save under the file menu and select "AOI layer as."
7. Select the data prep module from the main Imagine toolbar and select "subset image."
   - Follow the same procedures as listed above, but before hitting okay select the AOI button at the bottom.
   - Select the file option at the top and enter the name of the AOI file you created in step 6.
   - Hit okay and okay again.
8. This will create an image with only non-bedrock areas.

Appendix 6. Expert Systems Classification

Through analysis of the pixel spectra and unit signatures, bands that best differentiated the units were identified and the break points within these bands for each unit determined. Once this data had been collected an expert classifier was created through the knowledge engineer module. Flood units are in the left hand column, geomorphic characteristics are in the center column, and the corresponding remote sensing characteristics for those geomorphic units on the right.

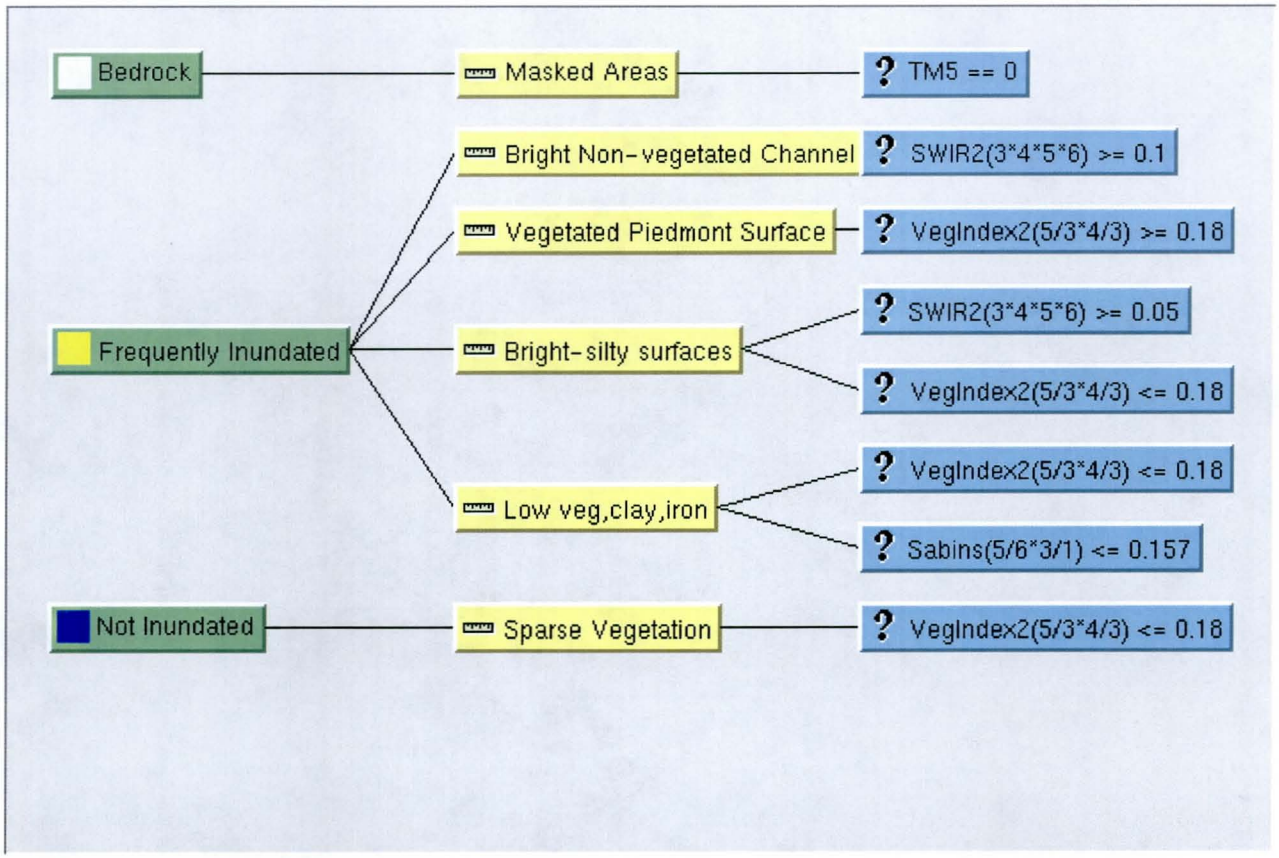

The expert classification file for Imagine is called floodunits4.ckb and is included on the CD-ROM disks included with this report.

Appendix 7: Additional explanation of some of the standard band ratios:

NDVI – *Figure A7.1*

Normalized Difference Vegetation Index which accentuates the presence and health of vegetation. A typical vegetation spectrum has moderate reflectance in band two giving it its green color, high reflectance in band 4 (near infrared) due to chlorophyll absorption. This ratio consists of (band 4-band3)/(band4 +band3) (Franklin et al., 1993). This calculation results in a new image in which the pixels range from -1 to 1, higher values indication green vegetation and low values indicating a lack of vegetation. In this ratio the active channels with vegetation such as palo verde are extremely bright indicating high amounts of vegetation. Also the high topographic areas, typically bedrock, show greater amounts of vegetation. The "darkest" feature in this image is the Hassayampa River active channel with has no vegetation and therefore has a very low DN value in this index.

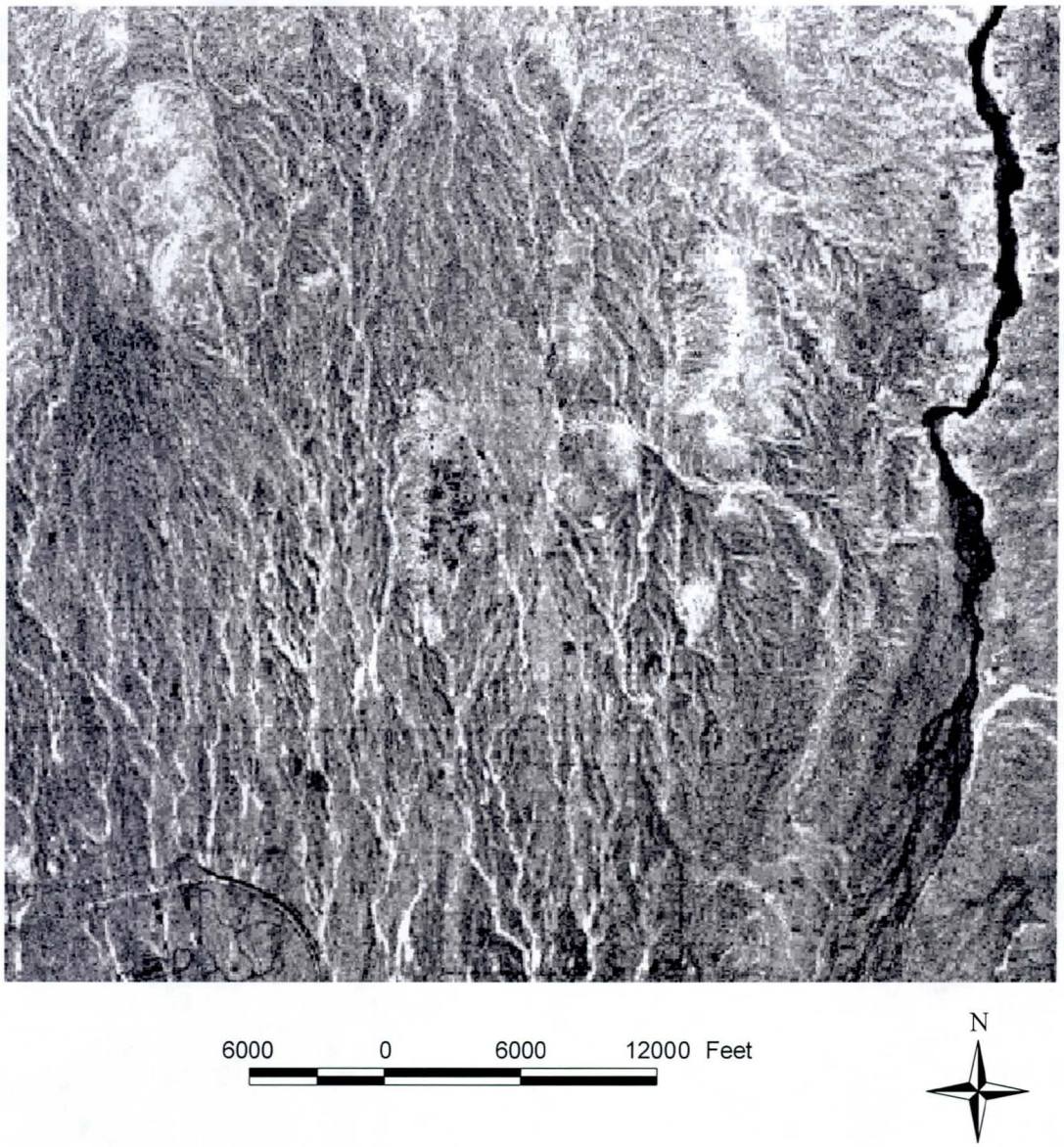

Figure A7.1. NVDI Image of Study Site

SAVI – *Figure A7.2*

Soil Adjusted Vegetation Index is used in arid and semi-arid regions where canopy cover of the ground surface is spotty and non-continuous. (Franklin, et al., 1993) This ratio adds a correction factor for soil to the standard NDVI: (4-3)*1.5/(4+3+1.5). The results of this ratio are almost identical to the NDVI ratio with piedmont channels and topographic high displaying as bright and the Hassayampa River displaying as dark.

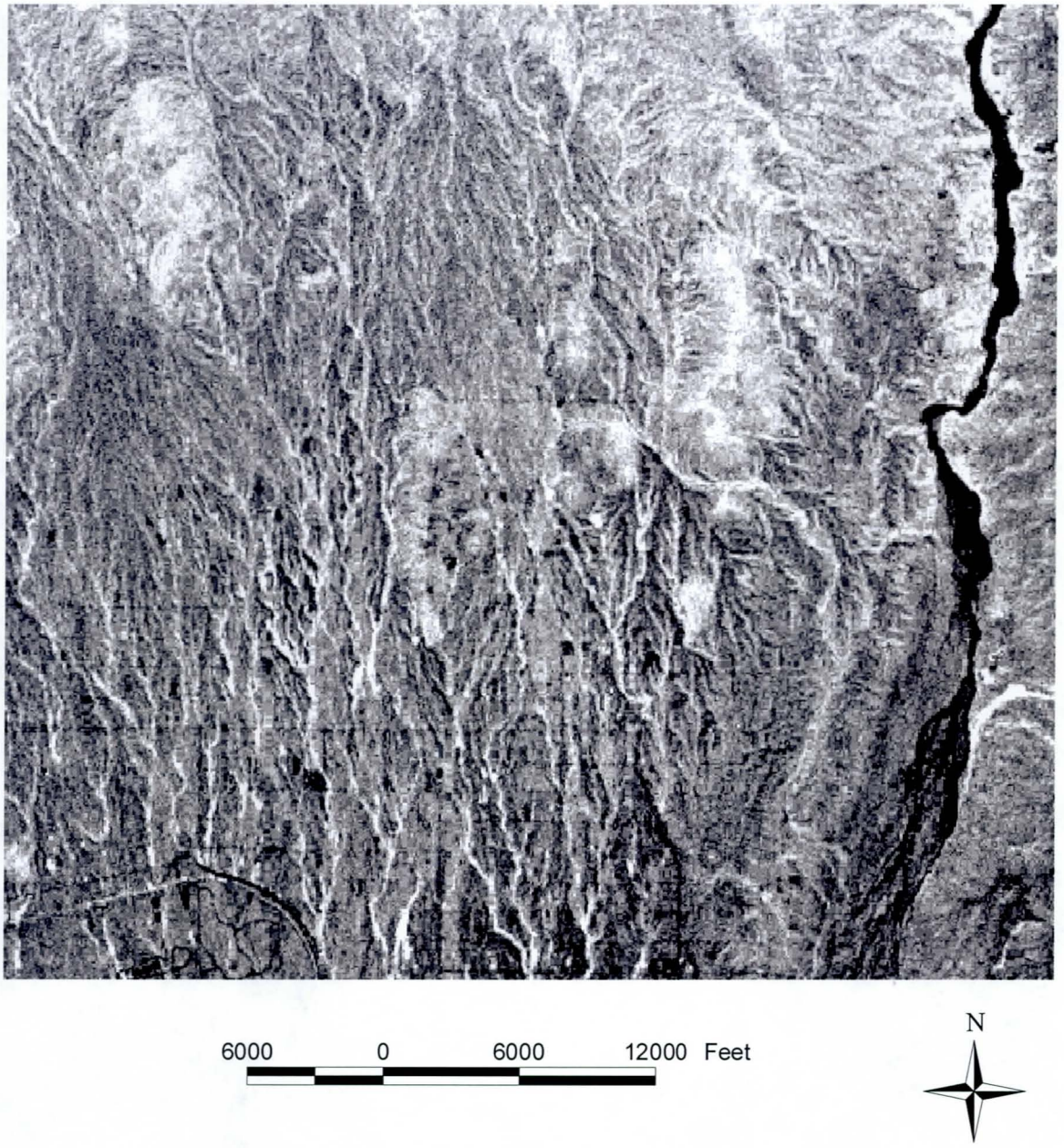

Figure A7.2. SAVI Image for Study Site

Hydroxyls/Clay ratio – *Figure A7.3*

The presence of hydroxyl ions produce an absorption feature in band 7, resulting in lower DN values where materials with hydroxyl ions are present. This ratio divides band 5 by band 7. Materials without hydroxyls will have values close to one, those with hydroxyl will have values greater than 1. Thus, brighter pixels have more hydroxyls than darker pixels. This has been dubbed the "clay ratio" as typically the material containing hydroxyl ions is a clay (Figure A7.3).

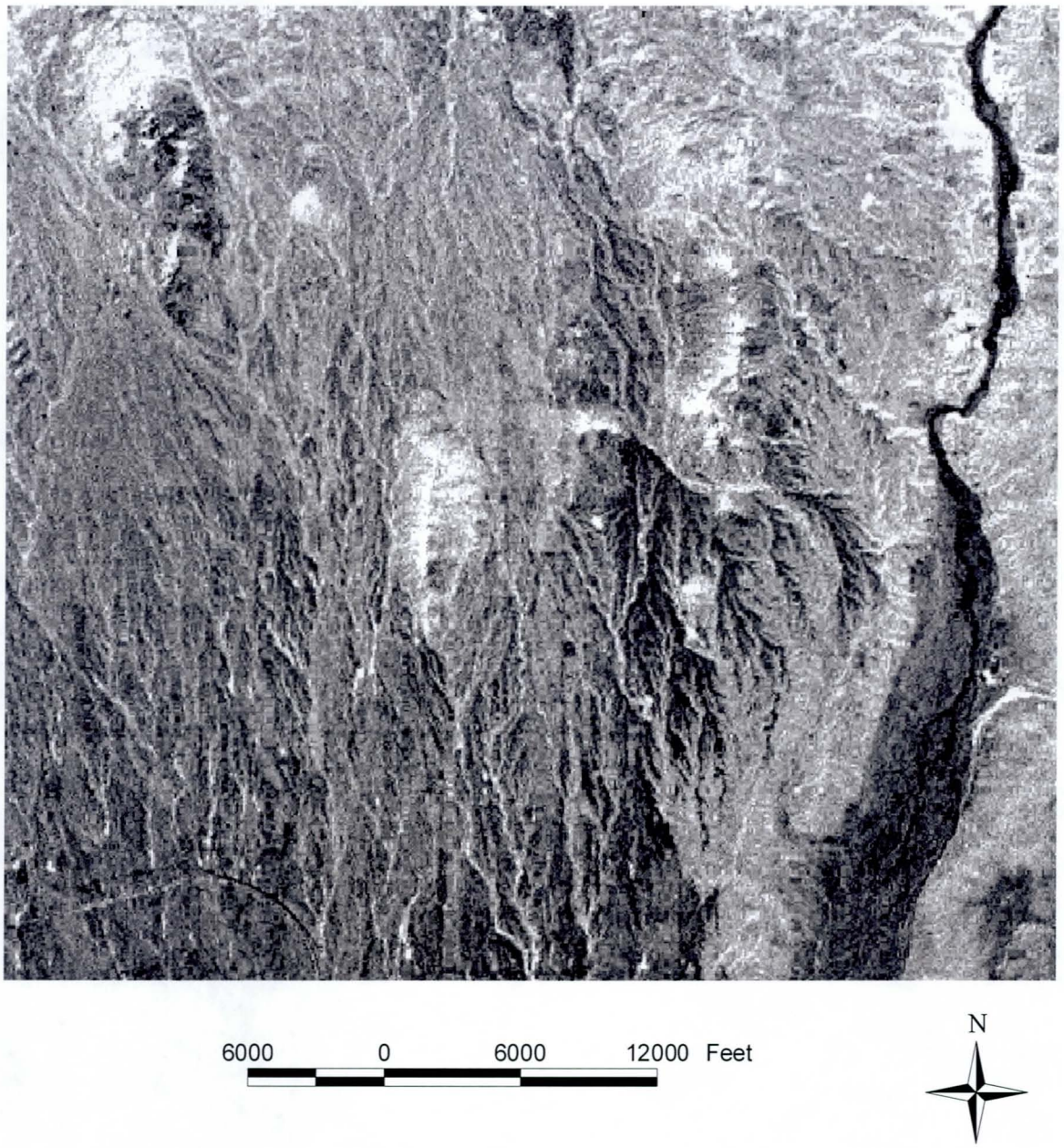

Figure A7.3 Clay Ratio Image for Study Site

This ratio illustrates one of the cautions in using indices. A ratio will not exclusively detect the feature it was designed to enhance; it will accentuate that material and any other that appear to have similar spectral features in the coarse Landsat spectra. In a lab spectra the two would probably not appear similar, but because Landsat has only 6 measurements, and a lab spectra hundreds, some

material can look similar in certain regions. In this particular case not only do hydroxyl ions have an absorption feature in band 7, but vegetation also has a lower band 7 value with respect to band 5. Thus, bright values in this ratio could indicate high clay contents or dense vegetation.

In the resulting image the older surfaces are darker, indicating either a higher clast to soil ratio or sparse vegetation. The more clast armoring, the less soil is present to the detector at the surface, resulting in a lower clay ratio value. The smaller active channels are bright in this image, not because of clay, but because of the dense vegetation.

Appendix 8. CD-ROM of digital data used and developed in this report